

A critical review of wheel/rail high frequency vibration-induced vibration fatigue of railway bogie in China

Vibration
fatigue of
railway bogie
in China

177

Xingwen Wu

School of Mechanical Engineering, Southwest Jiaotong University, Chengdu, China

Zhenxian Zhang

State Key Laboratory of Rail Transit Vehicle System, Southwest Jiaotong University, Chengdu, China

Wubin Cai

School of Mechanical Engineering, Southwest Jiaotong University, Chengdu, China

Ningrui Yang and Xuesong Jin

State Key Laboratory of Rail Transit Vehicle System, Southwest Jiaotong University, Chengdu, China

Ping Wang

Key Laboratory of High-speed Railway Engineering Ministry of Education, Southwest Jiaotong University, Chengdu, China

Zefeng Wen, Maoru Chi and Shuling Liang

State Key Laboratory of Rail Transit Vehicle System, Southwest Jiaotong University, Chengdu, China, and

Yunhua Huang

School of Mechanical Engineering, Southwest Jiaotong University, Chengdu, China

Abstract

Purpose – This review aims to give a critical view of the wheel/rail high frequency vibration-induced vibration fatigue in railway bogie.

Design/methodology/approach – Vibration fatigue of railway bogie arising from the wheel/rail high frequency vibration has become the main concern of railway operators. Previous reviews usually focused on the formation mechanism of wheel/rail high frequency vibration. This paper thus gives a critical review of the vibration fatigue of railway bogie owing to the short-pitch irregularities-induced high frequency vibration,

© Xingwen Wu, Zhenxian Zhang, Wubin Cai, Ningrui Yang, Xuesong Jin, Ping Wang, Zefeng Wen, Maoru Chi, Shuling Liang and Yunhua Huang. Published in *Railway Sciences*. Published by Emerald Publishing Limited. This article is published under the Creative Commons Attribution (CC BY 4.0) licence. Anyone may reproduce, distribute, translate and create derivative works of this article (for both commercial and non-commercial purposes), subject to full attribution to the original publication and authors. The full terms of this licence may be seen at <http://creativecommons.org/licenses/by/4.0/legalcode>

The author sincerely appreciates the help provided by the research team (Wheel/rail interaction, Vibration and Noise Research Team) and CRRC. In addition, this study has also been supported by Science and Technology Research Plan of China Railway General Corporation (No. P2019J002, N2022J009), China Association of Science and Technology Young Talent Support Project (No. 2019QNRC001), National Natural Science Foundation (No. U1934203), and Sichuan Science and Technology Program (No. 2022NSFSC0469, 2023NSFSC0374, 2023YFH0049).



including a brief introduction of short-pitch irregularities, associated high frequency vibration in railway bogie, typical vibration fatigue failure cases of railway bogie and methodologies used for the assessment of vibration fatigue and research gaps.

Findings – The results showed that the resulting excitation frequencies of short-pitch irregularity vary substantially due to different track types and formation mechanisms. The axle box-mounted components are much more vulnerable to vibration fatigue compared with other components. The wheel polygonal wear and rail corrugation-induced high frequency vibration is the main driving force of fatigue failure, and the fatigue crack usually initiates from the defect of the weld seam. Vibration spectrum for attachments of railway bogie defined in the standard underestimates the vibration level arising from the short-pitch irregularities. The current investigations on vibration fatigue mainly focus on the methods to improve the accuracy of fatigue damage assessment, and a systematical design method for vibration fatigue remains a huge gap to improve the survival probability when the rail vehicle is subjected to vibration fatigue.

Originality/value – The research can facilitate the development of a new methodology to improve the fatigue life of railway vehicles when subjected to wheel/rail high frequency vibration.

Keywords Wheel/rail high frequency vibration, Vibration fatigue, Railway bogie, Fatigue damage assessment

Paper type Literature review

1. Introduction

The railway bogie is a crucial component for rail vehicle and serves an important role in steering vehicle operating on the track and supporting loads from the car body. Therefore, the railway bogie is expected to be subjected to dynamic loads arising from wheel/rail interaction, car body motion, as well as traction and braking systems. These loads are usually characterized by the broadband frequency due to varying speeds, different track types and operational conditions, which pose a huge challenge for the vehicle design. In recent years, vibration fatigue, referred to as fatigue failure caused by random vibration especially when the excitation frequency is approaching the natural frequency of structural, has been widely reported by railway operators. These fatigue failures occurring in railway bogie are usually related to the wheel/rail high frequency impact and can pose highly adverse influences on operating safety. Therefore, this paper aims to elaborate the wheel/rail high frequency vibration, and the resulting vibration fatigue in railway bogie as well as the associated methodologies used to estimate vibration fatigue.

2. Wheel/rail high frequency vibration in railway bogie

The rail vehicle operates on two parallel rails through the wheel/rail rolling contact. The contact at the wheel/rail interface is characterized by large contact stiffness due to the steel-made wheel and rail, and the size of the contact patch is similar to the dimension of the thumb. Therefore, the contact force of wheel/rail interaction is very sensitive to irregularities at the wheel/rail interface. These irregularities could be from either the wheel or the rail interface. It has been reported that the short pitch irregularities of wheel/rail serve as the main resource of wheel/rail high frequency vibration (Tao, Wen, Jin, & Yang, 2020; Tao, Xie, Wang, Yang, Ding, & Wen, 2020), which are usually associated with the structural fatigue failure and wheel/rail noise emission, as shown in Figure 1. The short-pitch irregularities on the wheel and rail interface could be classified into discrete irregularities and periodic irregularities distributed on the wheel circumference and rail head. The discrete irregularities could consist of wheel flat, wheel shelling and wheel spalling on the wheel circumference, as well as the rail joint on the rail head. Those irregularities can give rise to a local impact at the wheel/rail interface. The wheel polygonal wear and rail corrugation are regarded as typically periodic irregularities at the wheel/rail interface, which can lead to high frequency and high magnitude impact for rail vehicles. Therefore, the wheel polygonal wear and rail corrugation-induced high frequency vibration are the main focus of this paper.

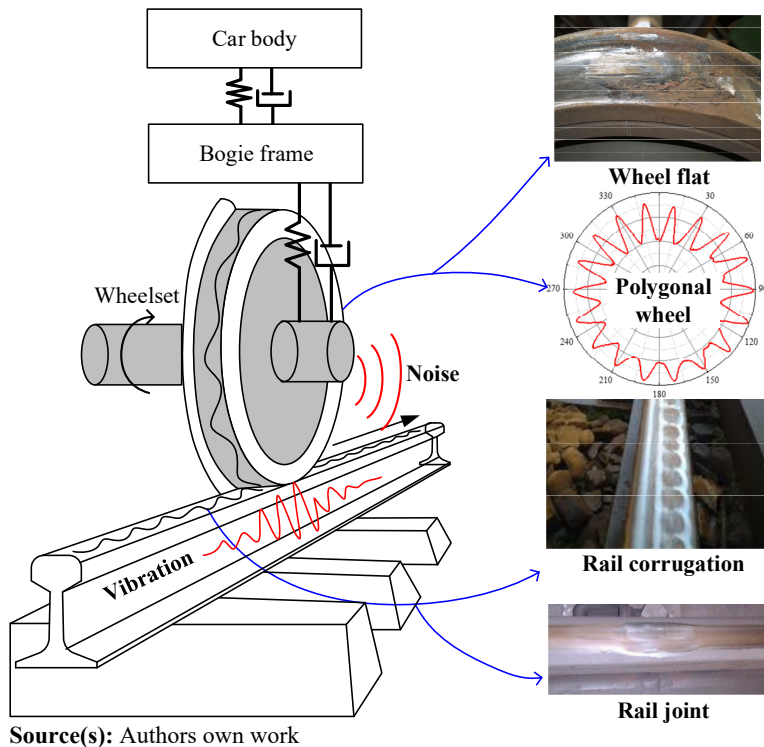


Figure 1.
Wheel/rail interaction
in the presence of short
pitch irregularities

2.1 Formation mechanisms of short-pitch irregularities

(1) Wheel OOR

The irregularities on the wheel circumference are also referred to as wheel Out-Of-Round (OOR). Due to its highly adverse influence, huge efforts have been made to understand the formation mechanism and its associated influence on high-speed rail vehicles, metro cars and locomotives. The most recent review on the formation mechanisms of wheel polygonal wear for high-speed rail vehicles, metro cars and locomotive were made by [Tao, Wen *et al.* \(2020\)](#), [Tao, Xie *et al.* \(2020\)](#), [Iwnicki, Nielsen, and Tao \(2023\)](#). The frequency-fixed mechanism is regarded as a general law for the formation of wheel polygonal wear, although the specific driving force of wheel polygonal wear still remains controversy for specific vehicles. The proposed formation mechanism of wheel polygonal wear includes the bending of wheelset ([Jin, Wu, Fang, Zhong, & Ling, 2012](#); [Tao, Wen *et al.*, 2020](#); [Tao, Xie *et al.*, 2020](#)), P2 resonance of wheel/rail ([Tao, Wen, Liang, Ren, & Jin, 2019](#); [Cai, Chi, Tao, Wu, & Wen, 2019](#)), rail localized bending between two wheelsets in a bogie ([Wu, Rakheja, Cai, Chi, Ahmed, & Qu, 2019](#); [Wu, Wu, Li, Shi, & Xu, 2019](#); [Cai, Wu, Chi, Yang, & Huang, 2022](#); [Qu, Zhu, Zeng, Dai, & Wu, 2020](#); [Ma, Gao, Cui, & Xin, 2021](#)), the structural resonance of bogie frame ([Wu, Du, Zhang, Wen, & Jin, 2017](#)), as well as the frictional self-excited vibration of wheelset-track system ([Zhao *et al.*, 2019](#); [Wu, Shang, Pan, Zhang, Shi, & Xiao, 2022](#); [Wu, Xie, Liu, Wu, Wen, & Mo, 2022](#)) and traction-induced wheelset torsional vibration and associated self-excited stick slip vibration ([Spangenberg, 2020](#)), as shown in [Figure 2](#). In addition, the initial irregularities on the wheel circumference ([Cai, Chi, Wu, Yang, & Huang, 2023](#); [Ye, Shi, Krause, Tian, & Hect, 2020](#); [Kang](#)

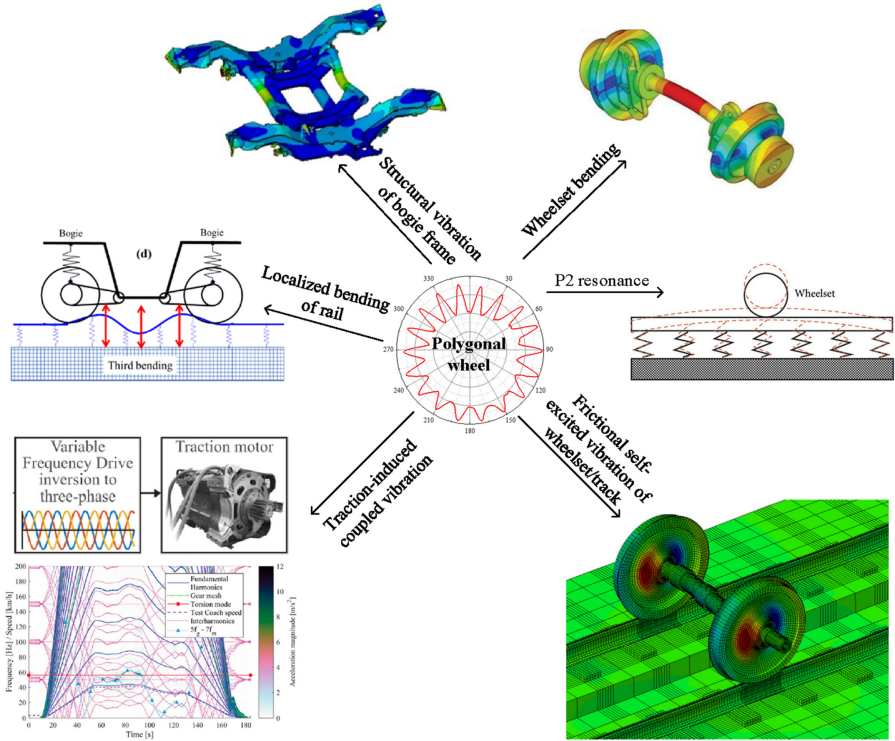


Figure 2. Typical formation mechanisms of wheel polygonal wear

Source(s): Authors own work

et al., 2022), wheelset flexibility (Peng, Iwnicki, Shackleton, Crosbee, & Zhao, 2019; Peng, Han, Chu, Gao, Liu, & Xiao, 2019) and traction (Chen *et al.*, 2023) can aggravate the formation of uneven wear on the wheel circumference.

It can be seen that the formation mechanisms of wheel polygonal wear are mainly attributed to the resonance of the natural vibration mode of the system, especially for the modes that affect the wheel/rail interaction. These suggest that the wheel polygonalization is a general wear process for rail vehicles, and a perfect round wheel could also tend to be an OOR wheel if the mitigation is not considered in the operation. Therefore, it is desirable to summarize the resulting excitation frequencies of polygonal wheel at the wheel/rail interface, which could facilitate the optimization of structure so as to avoid the exciting frequencies of polygonal wheels. Table 1 summarizes typical wheel polygonal wear and associated excitation frequencies for wheel/rail interaction reported by references. It can be seen the dominating excitation frequencies of polygonal wear for metro cars and locomotive mainly lies in the frequency band of less than 100 Hz approximately. Whereas for high-speed trains, the wheel polygonal wear-induced excitation frequency can reach up to 650 Hz, mainly ranging from 550 to 650 Hz.

(2) Rail corrugation

Rail corrugation is a periodic wear on the rail head. Grassie classified rail corrugation into six types: heavy haul corrugation, light rail corrugation, corrugation related to track form, corrugation caused by P2 resonance, flange-type corrugation and rail Pinned-Pinned

corrugation (Grassie, 2009). Zhai *et al.* and Wen *et al.* summarized the phenomenon, causes and countermeasures of rail corrugation in China's high-speed lines and metro lines, respectively (Zhai, Jin, Wen, & Zhao, 2020; Wen, Tao, Zhao, Wei, & Jin, 2023), as listed in Table 2. As pointed out by Jin *et al.*, rail corrugation exhibits diverse forms, and its formation mechanisms are highly complex (Jin, Li, Li, & Wen, 2016). The occurrence and development of rail corrugation are influenced by both the natural characteristics of the vehicle-track system, such as vehicle speed, un-sprung mass, rail pad spacing, fastener stiffness and damping and track slabs types, as well as the operating environmental conditions (e.g. straight track, curved track, roughness of the wheel-rail interface, wheel-rail friction efficiency) and the type of vehicles (heavy haul, light rail, etc.). Due to this diversity and complexity, it is challenging to summarize the growth mechanism of all corrugation phenomena using a single theory. Most rail corrugation is due to the periodic fluctuations in the wheel-rail interface (such as wheel-rail normal force and creepages), then lead to periodic fluctuations in wheel/rail wear depth and gradually accumulate into rail corrugation. There are many reasons for these periodic wheel-rail vibrations, such as resonance of the wheelset itself

Vehicle	Order, vehicle speed and formation mechanisms	Frequency
Metro car	9th order, 50–80km/h, First bending of wheelset	85 Hz
	13th order, 120km/h, First bending of wheelset	78–96 Hz
	5–8th order, 60 km/h, P2 resonance of wheel/rail	31–63 Hz
Locomotive	20th order, 40 km/h, resonance of a coupled traction motor pitching and axle torsional mode	60.4 Hz
	18\19\24 order, 80 km/h, bending of wheelset and wheel disc	84 Hz, 122 Hz
High-speed train	18–20th order, 300 km/h, Localized bending of rail in the length range of wheelbase	550–580 Hz
	25 order, 250 km/h, Localized bending of rail in the length range of wheelbase	595–650 Hz

Source(s): Authors own work

Table 1. Typical wheel polygonal wear and the associated excitation frequencies

Line	Wavelength, vehicle speed; track characteristics (reasons)	Frequency
Metro line	30–40 mm, 80–90 km/h; resilient fasteners (GJ-III)	556–833 Hz
	50–63 mm, 55–70 km/h; resilient fasteners (Cologne-Egg)	243–389 Hz
	40–50 mm, 83 km/h; resilient fasteners (Vanguard)	461–576 Hz
	100–250 mm, 40–50 km/h; conventional fasteners, Curve Radius <300 m	44–139 Hz
	200–250 mm, 65–70 km/h; conventional fasteners, 600 m < Curve Radius <800 m	72–97 Hz
	80–100 mm, 60–80 km/h; conventional fasteners, Rubber bootied short sleeper, 400 m < Curve Radius <700 m	167–278 Hz
	50 mm, 35–40 km/h; Type-II fasteners, Rubber bootied short sleeper, Curve Radius = 350	194–222 Hz
	125–200 mm, 60–80 km/h; conventional fasteners, Ladder-type sleeper, 400 < Curve Radius ≤600	83–178 Hz
	60–100 mm, 35–40 km/h; Type-II fasteners, Ladder-type sleeper, Curve Radius = 350	97–185 Hz
	High-speed line	60–80 mm, 300 km/h; pinned-pinned resonance
120–160 mm, 300 km/h; vertical bending mode of the rails		520–694 Hz
63–80 mm, 250 km/h; rail pre-grinding		868–1,102 Hz

Source(s): Authors own work, Wen *et al.* (2023)

Table 2. Typical rail corrugation and associated excitation frequencies

(Tassilly & Vincent, 1991; Vila, Baeza, Martínez-Casas, & Carballera, 2014; Torstensson & Schilke, 2013; Suda, Komine, Iwasa, & Terumichi, 2002; Fourie, Frohling, & Heyns, 2020), resonance of the track itself (Jin, Wen, Wang, Zhou, & Liu, 2006; Li *et al.*, 2016; Daniel, Horwood, Meehan, & Wheatley, 2008; Wu, 2011), wheel–rail contact resonance (Carson & Johnson, 1971), vehicle-track coupling resonance (Kurzeck, 2011; Wang & Wu, 2020) and self-excited vibrations of the wheel–rail system (Clark, Scott, & Poole, 1988; Chen *et al.*, 2020; Cai *et al.*, 2020), as shown in Figure 3. Similar to the wheel polygonal wear, the rail corrugation developed by dynamic cause also follows the frequency-fixed mechanism.

2.2 Wheel/rail high frequency vibration

Through the above-mentioned investigations, the wheel/rail short-pitch irregularities can lead to high frequency and high magnitude impact at the wheel/rail interface near the passing frequency, thereby intensified vibration level for rail vehicles. The wheel polygonal wear-induced impact can affect the whole wheel re-profiling cycle until the reprofiling process is performed. The rail corrugation usually affects the local track section when the vehicle passes through, especially for the tight curve section. Considering the highly adverse influence on the rail vehicles, huge efforts have been made to explore the short-pitch irregularities-induced high frequency vibration through both the tests and numerical simulations.

(1) Experimental investigations

The short-pitch irregularities-induced high frequency impact load can reach up to 1,000 Hz, which poses a huge challenge to measure impact loads arising from the wheel polygonal wear and rail corrugation through the instrumented wheelset. Therefore, the axle box acceleration is usually employed to quantify the influences of short-pitch irregularities on the vehicle in the tests. To capture the evolution of axle box acceleration from the new wheel to the worn wheel conditions, the long-term field test campaigns were usually conducted. Cai *et al.* conducted a long-term field test for a high-speed train operating at a speed of 250 km/h (Cai *et al.*, 2020). In the test, the tested vehicle was subjected to severe wheel polygonal wear with the harmonic order of 22–25th, which gives rise to obvious influences on the axle box

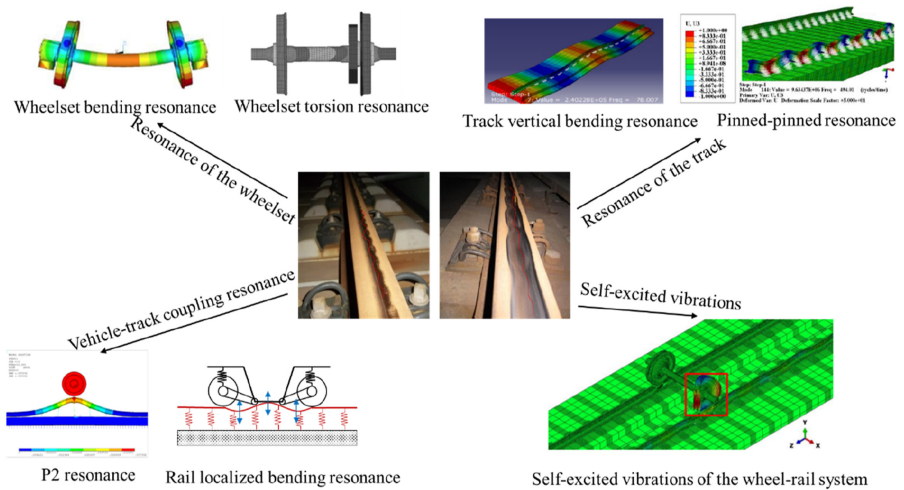


Figure 3. Typical formation mechanisms for rail corrugation

Source(s): Authors own work

acceleration (especially for the passing frequency band of 550–650 Hz), as shown in Figure 4. In the lateral stage of the wheel re-profiling cycle, the acceleration of the axle box showed a rapid increase with the vehicle mileages due to the wheel polygonal wear. The results also showed that the frequently varying speed can lower the increase rate of wheel polygonal wear. Wu *et al.* reported the evolution of wheel polygonal wear for a high-speed train operating at 300 km/h and pointed out that the maximum vertical acceleration of the axle box can reach up to 400 g due to severe wheel polygonal wear, and the associated impact can excite some high frequency vibration mode (up to around 1,000 Hz) near the double passing frequency of wheel polygonal wear (Wu, Rakheja, & Wu, 2018; Wu, Rakheja, & Qu, 2018). Moreover, the wheel polygonal wear-induced high frequency vibration is obviously greater than those defined in IEC 61373 (Wu *et al.*, 2023), especially for the dominating frequency band of wheel polygonalization (550–650 Hz), as shown in Figure 5. This suggests that the axle box vibration level given in IEC 61373 could underestimate the vibration level of the axle box in the presence of wheel polygonalization. These could significantly shorten the fatigue life of rail vehicles, thereby the occurrence of in-service fatigue failures.

Alternatively, some researchers investigated the wheel polygonal wear-induced high frequency vibration through a roller test rig. China Academy of Railway Sciences Corporation Limited developed a full-size roller test rig for a single wheelset so as to

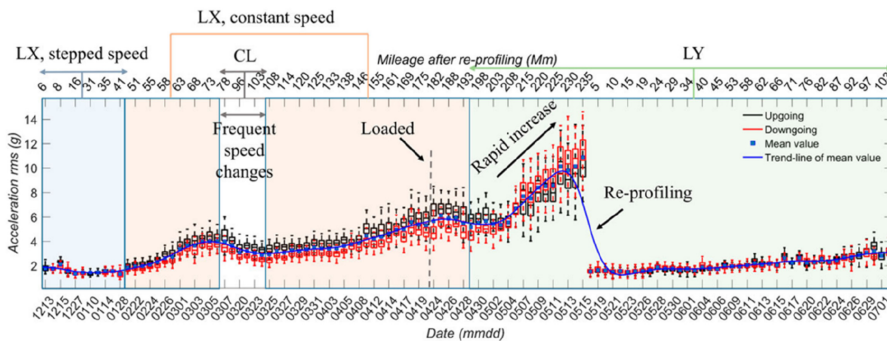


Figure 4. Evolution of RMS value for vertical axle box acceleration in terms of vehicle mileage

Source(s): Cai *et al.* (2020)

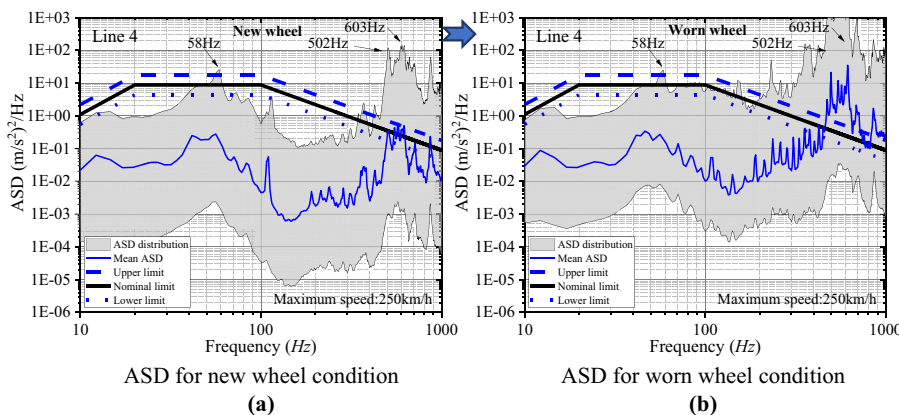


Figure 5. Comparison of axle box ASD spectra for new- and worn-wheel conditions

Source(s): Wu *et al.* (2023)

investigate the high frequency vibration of wheel/rail interaction (Chang, Cai, Chen, Li, & Lin, 2022), as shown in Figure 6. This test rig was employed to explore the wheel flat-induced impact at the wheel/rail interface (Wu, Chi, Liu, Hu, Liang, & Wen, 2020; Wu, Xie, Liu, Wu, Wen, & Mo, 2020) and the formation process of wheel polygonal wear (Wu, Shang *et al.*, 2022; Wu, Xie *et al.*, 2022). Similarly, Liu *et al.* utilized a full-scale roller test rig for a single wheelset incorporating with a numerical model to study the combined vibration of the wheelset and gear box arising from the wheel polygonal wear and track irregularity (Liu, Yang, & Liu, 2022), as shown in Figure 7. Although the considered wheel polygonal wear is limited to the

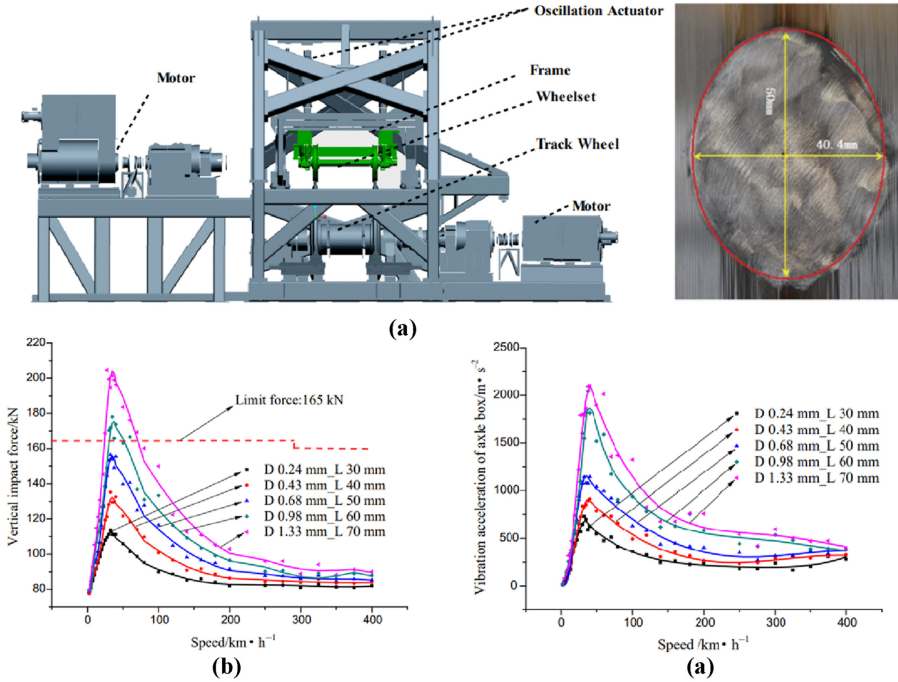


Figure 6. Experimental investigation on the wheel/rail interaction due to wheel flat, (a) roll test rig, (b) wheel flat-induced wheel/rail impact forces, and (c) axle box acceleration caused by wheel flat

Source(s): Chang *et al.* (2022)

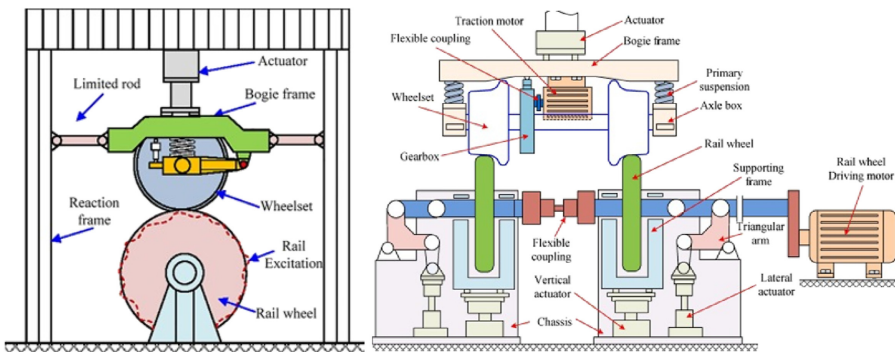


Figure 7. Full-scale roller test rig for a single wheelset

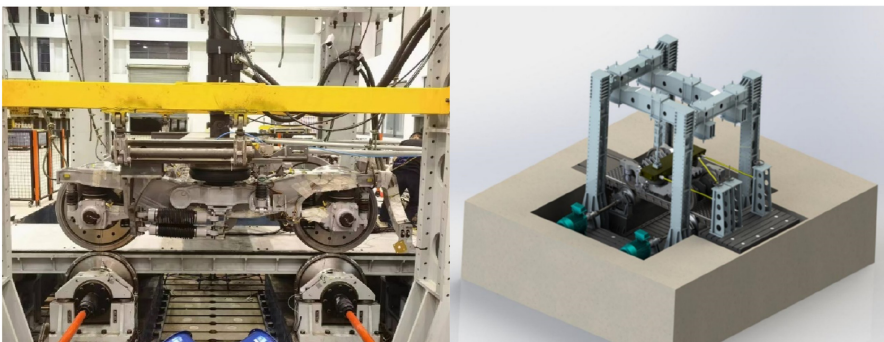
Source(s): Liu *et al.* (2022)

first-order OOR, the wheel polygonal wear-induced vibration is still identified as the main contributor for the vibration of wheelset. Similarly, Zhang *et al.* designed the roller as polygonal wheel with high-order polygonal wear to simulate the high frequency vibration of wheelset (Zhang, Ping, & Wu, 2018). To better simulate the high frequency vibration of bogie frame, Wu *et al.* developed a roller test rig for the whole railway bogie rather than a single wheelset (Wu, Chi *et al.*, 2020; Wu, Xie *et al.*, 2020), as shown in Figure 8, which enables us to identify the transfer path of high frequency vibration from the wheel/rail interaction to the bogie frame. Considering the limitations of hydraulic actuators for the high frequency loading, the above-mentioned test rigs serve as an alternative method to simulate the high frequency of wheel/rail interaction, although these test rigs are still subjected to limitations, such as regardless of the effects of track support stiffness which could overestimate wheel/rail impact load and axle box acceleration with respect to the real operating condition.

Rail corrugation is discretely distributed in the local region of track, especially in tight curves. It is known that the inner rail is subjected to larger wheel/rail creepage in the curve, therefore, the inner rail is much more vulnerable to rail corrugation with respect to the outer rail. The characteristics of rail corrugation are highly related to track properties, and the resulting dynamic responses could vary substantially in a single railway line due to different track types (Wu, Chi *et al.*, 2020; Wu, Xie *et al.*, 2020), as shown in Figure 9. The rail corrugation-induced axle box acceleration is significantly greater than those observed in the track section without rail corrugation. Moreover, the short sleeper track and rubber booted sleeper track yield different wavelengths for the rail corrugation, thereby different dominating frequencies (70 Hz for short sleeper track and 200 Hz for rubber booted sleeper track). In China, a railway line could consist of different damping track types (especially for metro lines) for different purposes of vibration reduction, thereby different characteristics for rail corrugation and exciting frequency for wheel/rail interaction, as listed in Table 2. The variations in the excitation frequencies of rail corrugation for different tracks pose huge challenges for the modal matching for the vehicle and track system, and the natural frequencies of rail vehicles cannot avoid all the exciting frequencies arising from the wheel/rail interaction, thereby leading to the vibration fatigue in the service.

(2) Theoretical investigations

In the theoretical study, the wheel polygonal wear and rail corrugation are generally modelled as a harmonic variation superposing on the wheel circumference or rail head (Li *et al.*, 2011; Liu & Zhai, 2014; Zhang *et al.*, 2014), which serves as a basic input for the simulation of vehicle and track model. From the interested frequency point of view, the vehicle and track system



Source(s): Wu, Chi, *et al.* (2020) and Wu, Xie, *et al.* (2020)

Figure 8.
Full-scale roller test rig
for a whole
railway bogie

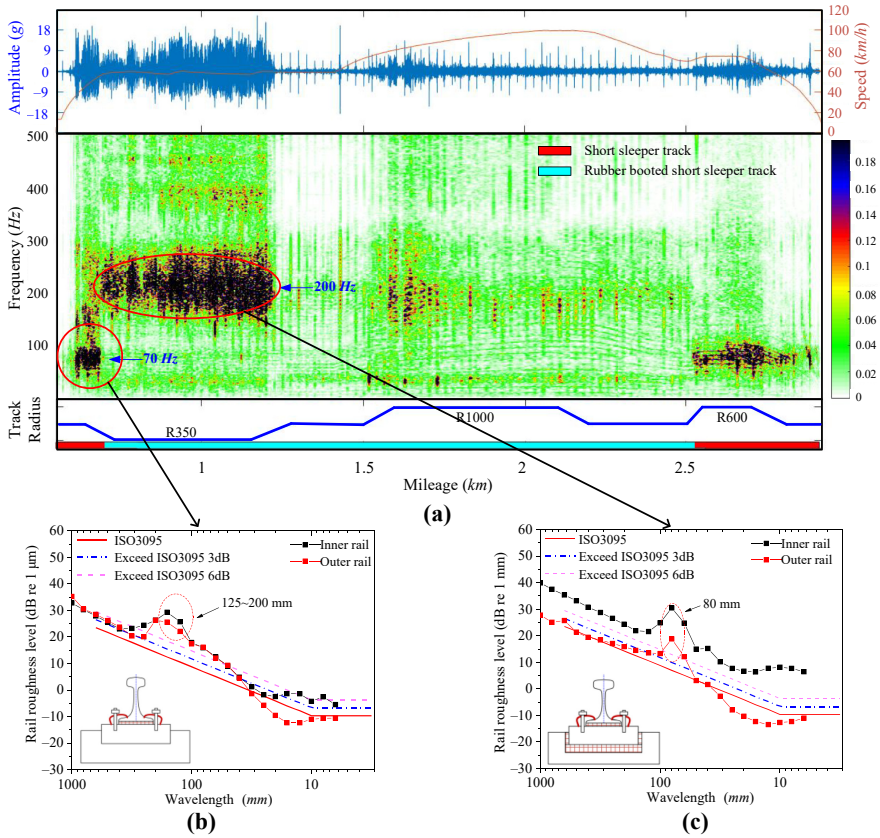
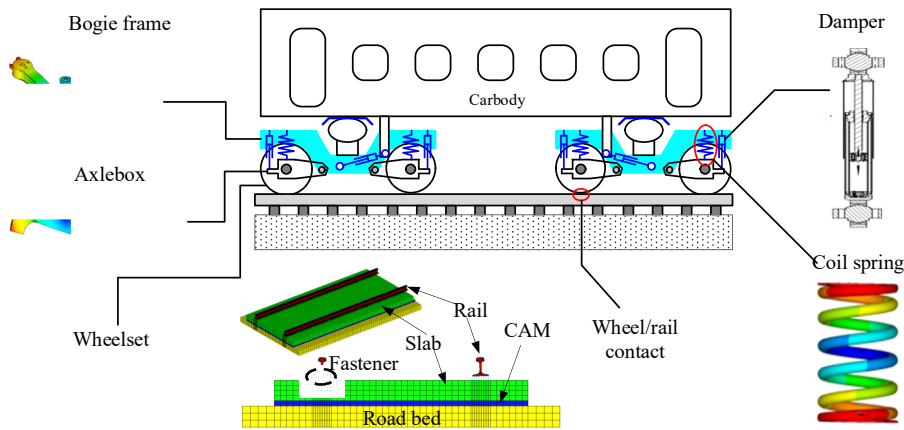


Figure 9.
Rail corrugation-
induced high
frequency vibration

Source(s): Wu, Chi, *et al.* (2020) and Wu, Xie, *et al.* (2020)

can be modelled in different frequency ranges, such as the mid-frequency range and the high frequency range. A review of modelling the vehicle and track system in the mid-frequency range 50–500 Hz was given by Popp *et al.*, in which the rail corrugation, deterioration of ballast or Out-Of-Round (OOR) wheel have been considered as main contributors to the mid-frequency oscillation in the railway system (Popp, Kruse, & Kaiser, 1991). Regarding to the wheel/rail noise problem, the high frequency vibration of the system up to 5,000 Hz is the interest. The related methods used to build the vehicle and track system in the high frequency range were reviewed by Knothe and Grassie (1993). In order to characterize the high frequency vibration arising from short-pitch irregularities, a vast number of models were developed on the basis of the theory of vehicle/track coupled dynamics (Zhai, Wang, & Cai, 2009) and the theory of rigid/flexible coupled dynamics. Dependent upon different purposes, the proposed models show varying complexities, including the flexibility in the rail, slab track, wheelset, axle box, coil spring, gear box and bogie frame, so as to consider the desired high frequency vibration (see Figure 10).

Through the simulation of a vehicle/track coupled dynamic model together with flexible models of interest components, the influences of short pitch irregularities have been widely investigated, in terms of wheel/rail normal force, wheel/rail creepage force, vibrations in the track, axle box, wheelset, gearbox, roller bearing, coil spring and bogie frame, as well as



Source(s): Authors own work

Figure 10. Vehicle/track coupled models considering varying complexities

dynamic stress arising from the high frequency vibration. Through simulation of a vertical coupled vehicle/track model along with the measured wheel polygonal wear, Liu and Zhai concluded that the damping effects of the wheel/rail interaction can impose a significant influence on the fluctuations of wheel/rail contact forces in the presence of wheel polygonalization, and the peak wheel/rail contact force always occur at the raising slopes of radius (Liu & Zhai, 2014), which was comparable with observed by Morys (1998). Considering a 20th-order wheel polygonal wear, Wu *et al.* investigated the influences of vehicle speed and polygonal wear amplitude on the wheel/rail normal force, axle box acceleration and stress of wheelset axle (Wu, Rakheja, & Wu, 2018; Wu, Rakheja, & Qu, 2018). The results demonstrated a nearly linear increase in the wheel/rail contact forces with wear amplitude. The high magnitude and high frequency impact loads owing to wheel polygonalization can excite some bending modes of vehicle and track subcomponents and further contribute considerably to the reduction of fatigue lifetime. Wu *et al.* investigated the dynamic stress developed in the wheelset axle shaft arising from the impact loads due to the wheel flat and wheel polygonalization through a coupled vehicle/track dynamic model along with a rotating flexible wheelset (Wu, Chi, & Wu, 2015). The results suggested that the wheel polygonalization can impose a significant influence on the dynamic stress in the wheelset axle shaft, and the secondary bending vibration mode of wheelset axle shaft could be excited by the wheel polygonalization-induced impact load. Yang *et al.* investigated the effects of wheel polygonal wear of locomotive on the wheel/rail creep forces and concluded that the anti-slip controller could contribute to the development of wheel polygonal wear (Yang, Xu, Ling, & Zhai, 2022). Moreover, a number of investigations focused on the effects of wheel polygonal wear on dynamic responses of roller bearing of axle box (Liao *et al.*, 2022; Wang *et al.*, 2019), torsional vibration of transmission system (Wang, Cheng, Mei, Zhang, Huang, & Yin, 2020; Wang, Xie, Jiang, Song, Sun, & Wang, 2020; Wang, Bai, Wu, Zheng, & Zhou, 2020) and gear box (Wu, Rakheja *et al.*, 2019; Wu, Wu *et al.*, 2019).

Regarding the rail corrugation-induced impact, Wu *et al.* developed a flexible bogie model incorporating an antenna beam and concluded that rail corrugation-induced high frequency vibration near 78 Hz can excite the coupled vibration of bogie frame and antenna beam thereby the intensified stress level (Wu, Shang *et al.*, 2022; Wu, Xie *et al.*, 2022). Zhou *et al.* reported the failure mechanism of coil spring through the simulation of vehicle/track model incorporating a flexible coil spring model and pointed out that the natural vibration mode of coil spring can be excited by the rail corrugation (Zhou *et al.*, 2020). In the above

investigations, the track was invariably considered as a tangent line. Considering a curved track, Bethel *et al.* developed a tram/track coupled model to study the effect of wheel polygonal wear on the dynamics of vehicle when negotiating a curve (Bethel *et al.*, 2022).

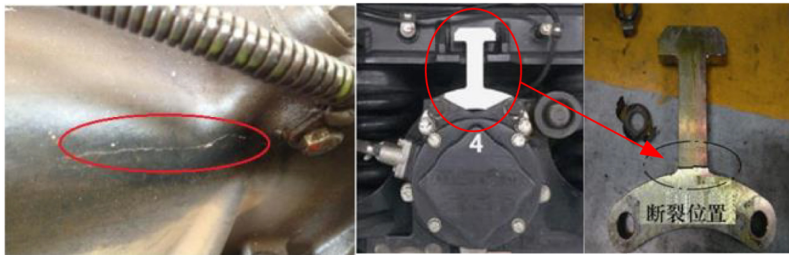
3. Wheel/rail high frequency vibration-induced vibration fatigue of railway bogie

The intensified vibration of railway bogie is expected to deteriorate the loading conditions thereby shortening the fatigue life of rail vehicles. Table 3 and Figure 11 summarized some typical fatigue failures of railway bogie reported by references, including the high-speed railway vehicles and metro vehicles. The well-known fatigue failure caused by the wheel OOR is the failure of the resilient wheel for IEC train, and the identified main causal factor is the low-order wheel polygonal wear-induced impact at the wheel/rail interface. After that, the wheel polygonal wear-induced vibration became a main concern for the structural integrity. In China, Zhang, Tan, and Lin (2016) and Hu, Liu, Liu, and Hai (2017) reported the fatigue failure of gear box in high-speed rail car and concluded that the failure of gear box was highly related to the structural resonance caused by wheel OOR. The experimental results showed that the wheel circumferential roughness was predominated by 20th-order wheel polygonal wear, and the resulting high frequency impact at the wheel/rail interface near 580 Hz can excite the vibration modes of the gear box, thereby the reduced fatigue life for the gear box. Similarly, the brake disc mounted on the wheelset axle have been also reported to be subjected to fatigue failure due to the combined effects of high frequency vibration and thermal loading in the braking process (Jin *et al.*, 2020). Through the field test, Peng *et al.* pointed out that the failure of the vertical block was related to the high order wheel polygonal wear-induced high frequency impact at the wheel/rail interface (Peng, Iwnicki *et al.*, 2019; Peng, Han *et al.*, 2019). Besides, the high-level vibration arising from the wheel polygonal wear can also give rise to the non-linear vibration in the axle box front cover of high-speed train and further contribute to the failure of connecting bolts (Feng, Qu, Li, Dai, & Shu, 2023). Dong *et al.* reported the failure of the wire bracket installed on the axle box through the field test and numerical simulation and concluded that the crack initiated from the weld defect and the combined impacts due to wheel polygonal wear and rail corrugation serve as the main driving force for fatigue failure (Dong, Wang, Dai, & Li, 2023).

Vehicle	Failed components	Causal factors	Characteristic frequency band
High-speed train	Gearbox	20th-order wheel polygonal wear	580 Hz
	Brake disc	20th-order wheel polygonal wear	580 Hz
	Axle box bolts	20th-order wheel polygonal wear	580 Hz
	Vertical block of axle box	25th- to 27th-order wheel polygonal wear	510 Hz
Metro cars	Wire bracket	15th to 22nd-order wheel polygonal wear	400–800 Hz
	Motor installation of bogie frame	8th-order wheel polygonal wear and rail corrugation with the wavelength of 206–417 mm	56.6–62.5 Hz
	Side frame of bogie	14th- to 16th-order wheel polygonal wear and rail corrugation	71, 89, 94 Hz
	Coil spring	Rail corrugation	60 Hz
	Antenna beam	Rail corrugation (wavelength 125–200 mm)	60–80 Hz
	Safety hanger of axle box	Rail corrugation (wavelength 61.5 mm)	258 Hz
	Lifeguard	Rail corrugation	63 Hz

Table 3. Typical fatigue failures of rail vehicles arising from high frequency vibrations

Source(s): Authors own work



Gearbox Zhang *et al.* (2016)

(a)

Safety hanger of axle box Shi *et al.* (2019)

(b)



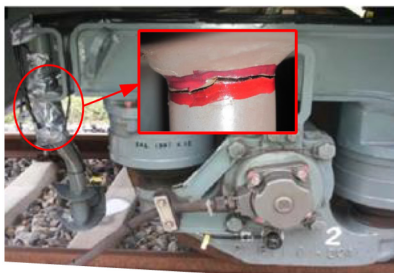
Bogie frame Wang *et al.* (2020)

(c)



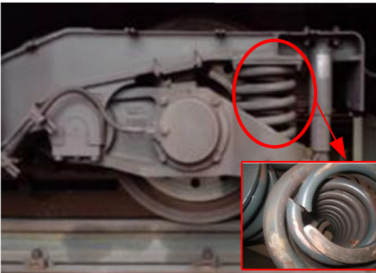
Antenna beam Wu *et al.* (2020)

(d)



Lifeguard Li *et al.* (2019)

(e)



Coil spring Zhou *et al.* (2020)

(f)

Source(s): Authors own work

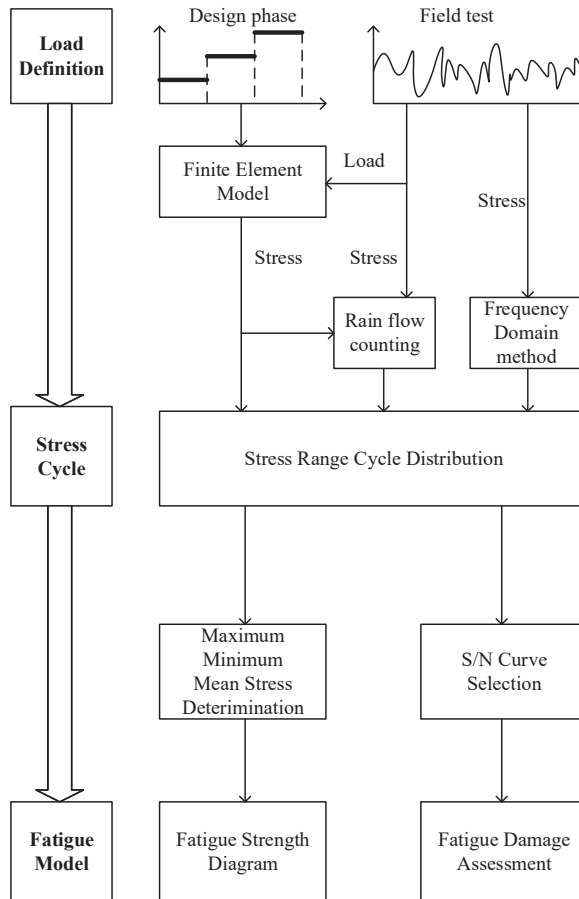
Figure 11. Typical fatigue failures caused by high frequency vibration of wheel/rail

Regarding metro cars, Wang, Cheng *et al.* (2020), Wang, Xie *et al.* (2020) and Wang, Bai *et al.* (2020) reported the fatigue failures of bogie frame through the field test, and the combined impacts due to the wheel polygonal wear and the rail corrugation were identified as the main contributor of fatigue failure of bogie frame. Zhou *et al.* (2020) and Ling *et al.* (2017) studied the fatigue failures of coil springs in a metro car and pointed out that the passing frequency of rail corrugation near 60 Hz can excite some vibration modes of coil spring. Through the field test and numerical simulation, Wu *et al.* concluded that the coupled bending mode between the bogie frame and antenna beam can be excited by the high frequency impact near 78 Hz arising from the rail corrugation (Wu, Chi *et al.*, 2020; Wu, Xie *et al.*, 2020). Li *et al.* studied the vibration fatigue of lifeguard in a metro car and concluded that the rail corrugation-induced

high frequency impacts excite the natural frequency of lifeguard thereby reducing fatigue lifetime (Li *et al.*, 2019). Shi *et al.* pointed out that the fatigue failure of the safety hanger is mainly attributed to the rail corrugation with the dominating wavelength of 61.5 mm (Shi, Wang, Dai, & Wu, 2019). Based on the aforementioned investigations, it is concluded that the axle-mounted components are much more vulnerable to fatigue failures compared with other components. The fatigue crack usually initiates from the defect of weld seam, and the wheel/rail high frequency impact-induced structural resonance serves as the main driving force of the failure of vehicle sub-components.

4. Methodologies used for assessment of vibration fatigue

The fatigue damage is usually employed to quantify the influences of service loads on the fatigue life of considered components. Therefore, this part focuses on methodologies used to assess the fatigue damage in both the design and service phases, especially focusing on load definitions and fatigue damage assessment models, as shown in Figure 12.



Source(s): Authors own work

Figure 12.
Basic flowchart of
fatigue assessment

4.1 Load definitions

(1) Main load for railway bogie frame

A number of international standards have been developed to specify the load spectrum of railway bogie, such as UIC515-4, UIC615-4, EN 13749, JIS E 4207 and JIS E 4208. UIC615-4 and UIC515-4 were defined by the International Union of Railways for motor bogie and trailer bogie of passenger rolling stock, respectively. Based on the track conditions in Europe, European countries developed EN 13749 according to the loads given in UIC standards. However, EN standard gives a more detail definition for longitudinal loads of bogie frame, such as the longitudinal lozenging force and potential shock. In those standards, the loads are classified into three types, such as exceptional loads, particular in-service loads and fatigue loads. Considering different operation conditions, the loads given in each standard are different. Japanese standards association developed JIS E 4207 and JIS E 4208 standards to verify the strength of bogie frame. To demonstrate the effects of difference of load definition, a number of investigations compared the fatigue results obtained from different methods. An *et al.* investigated the methodologies of fatigue assessment given in the JIS standard and further compared with UIC and EN standards and concluded that the JIS standard gave a more detail definition for the operational loads of bogie frame compared with other standards, whereas the exceptional load conditions are not defined in JIS standard (An, Li, Huang, Fu, & Yu, 2009). Liu *et al.* investigated the fatigue strength of a metro bogie frame and concluded that the JIS standard yields more conservative results for the fatigue strength of the weld seam of bogie frame compared with the UIC standard (Liu, Yang, Xiao, Yang, & Zhu, 2019).

It is known that the load spectrum is the basic input for verification of fatigue strength of railway bogie, and it is significantly affected by vehicle conditions and interfaces, operational characteristics, line characteristics and environmental conditions, and so on. The loads given in the current standards thus could be subjected to limitations due to differences in the operation condition of China railway. Therefore, it is of great interest to explore the load spectrum of bogie through field tests. In China, huge efforts have been made to understand the load spectrum of railway bogie, especially for new modes of high-speed rail vehicles, through the development of load cells for bogie frame, coil spring, axle box, traction rad, braking and wheelset, as shown in Figure 13.

Zhang *et al.* proposed a methodology to establish the load spectrum of bogie frame for a high-speed train based on the criteria of damage consistency method, which was used to measure the load spectrum of bogie frame operating at a speed of 350 km/h on the Jin-Jin high-speed railway line (Zhang, 2008). Ren *et al.* developed an instrument coil spring to measure dynamic loads of coil springs through a field test and pointed out that the maxima load mainly occurs at the entrance of the depot and railway connection section (Ren, Sun, & Li, 2010). Wang *et al.* developed the coil spring and axle box as load sensors with a validated frequency of up to 50 Hz, so as to measure the vertical and lateral forces acting on the bogie frame in the operation condition (Wang *et al.*, 2015). The obtained loads were further employed to calculate the bounce, roll, torsion and lateral load spectrum of bogie frame. The results concluded that the wheel reprofiling process can effectively reduce lateral loads of axle box, up to 50% and 40% for the tangent and curve sections, respectively. Ren *et al.* proposed a method to identify the traction and braking loads and concluded that the traction and braking forces were highly related to the traction and braking process, irrespective of curve negotiation (Ren, Zhao, Li, Wang, & Wu, 2022). Zou *et al.* conducted a comprehensive load calibration experiment for a bogie frame to identify the service load conditions of bogie frame (Zou *et al.*, 2016, 2021). The damage consistency criterion was subsequently used to develop the load spectrum of bogie frame.

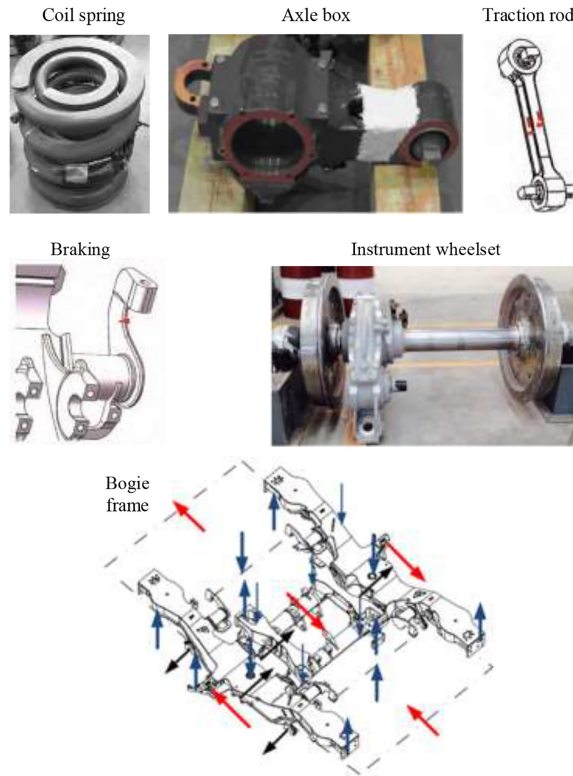


Figure 13.
Calibrated load cell for
components of
railway bogie

Source(s): Authors own work

In the aforementioned investigations, a linear relationship between the load and the stress was usually established through the laboratory test based on the quasi-static method, so as to identify the load through the stress developed on the structure. In the operation, the bogie frame is usually subjected to multiple dynamic forces. Therefore, the relationship between the stress and force can be further derived as:

$$\left\{ \begin{array}{l} S_1 = F_1k_{11} + F_2k_{12} + \dots + F_nk_{1n} \\ S_2 = F_1k_{21} + F_2k_{22} + \dots + F_nk_{2n} \\ \vdots \\ S_m = F_1k_{m1} + F_2k_{m2} + \dots + F_nk_{mn} \end{array} \right. \Rightarrow \mathbf{S}_m = \mathbf{K}_{mn}\mathbf{F}_n \quad (1)$$

where \mathbf{S}_m is the stress matrix which is a measurement obtained in field tests, \mathbf{K}_{mn} is the force–stress transfer matrix obtained in the calibration experiment by applying the unit force for each loading location, and \mathbf{F}_n is the desired dynamic forces. In this method, the location of stress gauge has to be selected carefully so as to omit the coupling effect of multiple forces, and the wheatstone bridge is usually employed in the calibration. This method is capable of identifying low frequency dynamic loads of bogie frame because the effects of mode vibration

of bogie frame on the stress are not taken into consideration. The main loads of bogie frame are mainly induced by the low frequency motion of car body, therefore, the quasi-static based instrument bogie frame could be considered acceptable for main load identification for a railway bogie frame. The methodologies used to identify the high frequency loads of railway bogie frame under the service condition still remain the challenge for the load definition of the railway bogie frame.

(2) Vibration spectrum for attachments of railway bogie

Unlike the main structure of a railway bogie, the attachments of bogie frame are mainly subjected to inertial loads arising from random vibration. EN 13749 defined the inertial accelerations for attachments installed on the axle box and bogie frame, respectively, as listed in Table 4. The proposed inertial is mainly limited to the magnitude of acceleration irrespective of exciting frequency, which could underestimate influences arising from the vibration fatigue. IEC 61373 standard defined a flat spectrum of ASD for bogie frame- and axle box-mounted components for both functional- and the simulated long-life vibration test, which has been employed to verify the structural integrity due to the random vibration. Figure 14 illustrates the typical load spectrum for axle box-mounted components given in IEC 61373. The cut-off frequency f_2 is taken as 500 Hz for the mass less than 50 kg, and 200 Hz for the mass greater than 125 kg. When the mass lies in the range from 50 to 125 kg, the cut-off

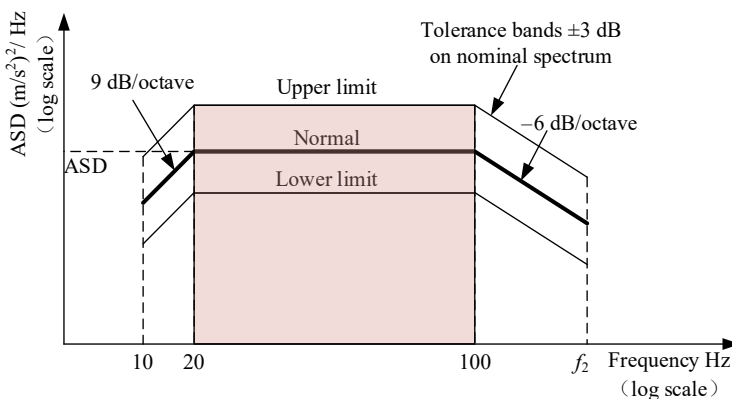
Direction	Axle box-mounted equipment		Bogie frame-mounted equipment	
	Exceptional acceleration	Fatigue acceleration	Exceptional acceleration	Fatigue acceleration
Vertical+	$\pm 70g$	$\pm 25g$	$\pm 20g$	$\pm 6g$
Lateral+	$\pm 10g$	$\pm 5g$	$\pm 10g$	$\pm 5g$
Longitudinal	$\pm 10g$	$\pm 5g$	$\pm 3g$ or $\pm 5g^*$	$\pm 2.5g$

Note(s): ⁺The values in the table apply to the bogie frame above the primary suspension. They may be reduced linearly to half the value at the bogie centre and should be extrapolated to higher values outboard of the primary suspension

*The value to be used depends on the type of bogie and application and should be consistent with the longitudinal shunt cases

Source(s): Authors own work

Table 4. Typical accelerations for equipment mounted on bogie frame and axle box in EN 13749



Source(s): Wu *et al.* (2023)

Figure 14. ASD spectrum of axle box-mounted components defined in IEC 61373 standard

frequency f_2 is calculated though 125×200 Hz/mass. The vibration spectrum is taken as a flat spectrum in the frequency range of 20 ~100 Hz. Whereas for the frequency range of 10 to 20 Hz and 100 ~ f_2 Hz, the slopes of 9 dB/octave and -6 dB/octave are considered for the ASD spectrum, respectively.

The functional vibration spectrum is the minimum vibration level to demonstrate that the equipment is capable of functioning when subjected to conditions that are likely to occur in service. The *RMS* values of the functional vibration spectrum in the vertical, transverse and longitudinal directions given by IEC 61373 are 38, 34 and 17 m/s^2 , respectively. Whereas the simulated long-life test aims at demonstrating the mechanical integrity of equipment at an increased vibration level, which is usually determined based on the vibration level of the functional vibration spectrum together with an acceleration ratio. In IEC 61373, the acceleration ratio is taken as 3.78 for the axle-mounted components, which permits us to simulate 25 years of fatigue lifetime for equipment in 15 h considering 5 h for each direction. Therefore, the *RMS* values of the simulated long-lifetime test are determined as 144, 129 and 64.3 m/s^2 for the vertical, transverse and longitudinal directions, respectively.

It can be seen that the axle box ASD spectrum given in IEC 61373 mainly consists of three interest frequency bands, and the vibration level in the frequency band of 20–100 Hz is taken as a flat spectrum. This suggests that the vibration spectrum of axle box defined in IEC 61373 aims to simulate the vibration level of a rail vehicle in the frequency band of 20–100 Hz and considers that this frequency band predominates the vibration level of axle-mounted components in the operation. However, in the operation, the vibration of axle box is predominated by multiple frequency bands rather than a single frequency band alone (Cai *et al.*, 2021; Wu *et al.*, 2017; Wu, Shang *et al.*, 2022; Wu, Xie *et al.*, 2022). Through analysing field test measurements obtained from nine high-speed railway lines, Wu *et al.* pointed out that the ASD spectrum in IEC61373 mainly focuses on the low frequency range of 20–100 Hz (Wu *et al.*, 2023). This can represent the overall vibration level of 20–100 Hz, whereas still underestimates the vibration level near the frequency of wheel/rail coupled mode (P2 force). The worst underestimations were observed for the frequency band of 500–700 Hz, especially for the high-speed train in the presence of wheel polygonal wear. Therefore, a multi-characteristic frequency bands-based axle box ASD vibration spectrum was proposed based on the distribution of wheel/rail coupled vibration modes in order to better characterize the vibration level of rail vehicles, as shown in Figure 15. The vibration level for each concerned frequency band is determined depending upon the distribution of *rms* values.

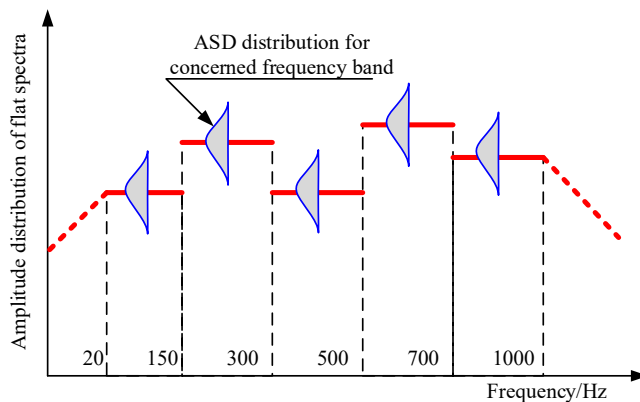
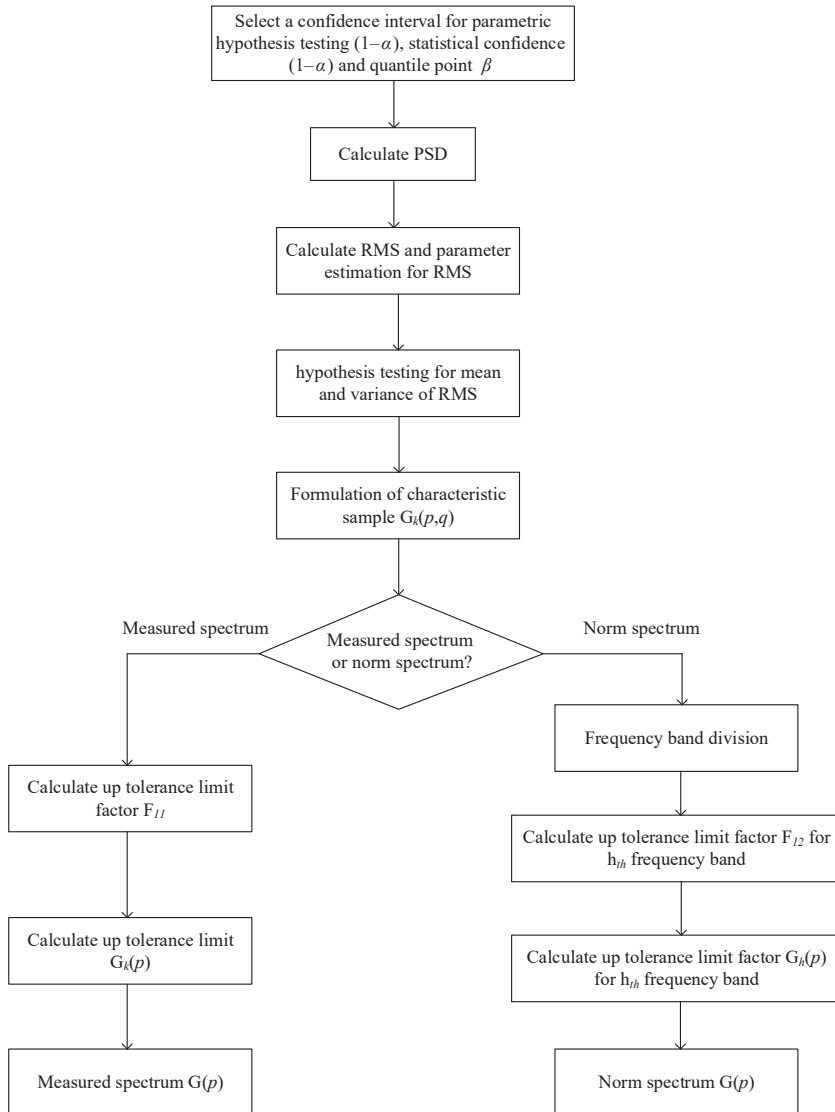


Figure 15.
Multi-characteristic
frequency bands-based
axle box ASD
spectrum

Source(s): Wu *et al.* (2023)

A few investigations have been made to synthesize the vibration spectrum based on the field test measurement through statistical synthesis methods, such as the vibration test specifications for flight vehicles (Klein & Piersol, 1965) developed by NASA, and the associated criteria for dynamic vibration test (Keegan, 2001; Himelblau, Piersol, Wise, & Grundvig, 1994; Angeli, 2016; MIL-STD-810F, 2008). Wange *et al.* conducted a comprehensive review of induction methods used in the aircraft vibration test data (Wang, Bai, Wan, & Yan, 2011). GJB/Z 126-99 defines a detailed procedure to synthesize the vibration spectrum for military vehicles, as shown in Figure 16. This method could be employed in railways for the induction of vibration spectrum. Upon the method



Source(s): Authors own work

Figure 16. Basic procedure for vibration induction given in GJB/Z 126-99

given in the standard, Ding *et al.* performed a vibration spectral induction for the onboard equipment of rail vehicles (Ding, Zhang, & Wang, 2016). Considering the strong non-normality of data in the railway vehicles, Deng *et al.* used the Johnson's law to improve the standard method of vibration induction (Deng *et al.*, 2019). A similar investigation was also conducted by Han *et al.* (2021). In the abovementioned investigations, the vibration data are inevitably considered as a Gaussian distribution; however, the vibration of railway vehicles expresses strong non-Gaussian characteristics, especially for the vibration of axle box due to random excitations at the wheel/rail interface.

4.2 Evaluation models of vibration fatigue

(1) Endurance strength method

In the current standards, the verification of the strength of railway bogie is based on the endurance strength method. The Goodman–Smith diagram and Goodman–Haigh diagram are usually employed to verify the fatigue strength of railway bogie. ERRI B 12/RP 17 defined the permissible stress for three types of steel using Goodman–Smith diagram in terms of the tensile strength (as shown in Figure 17), including the tensile strength of at least 370, 420 and

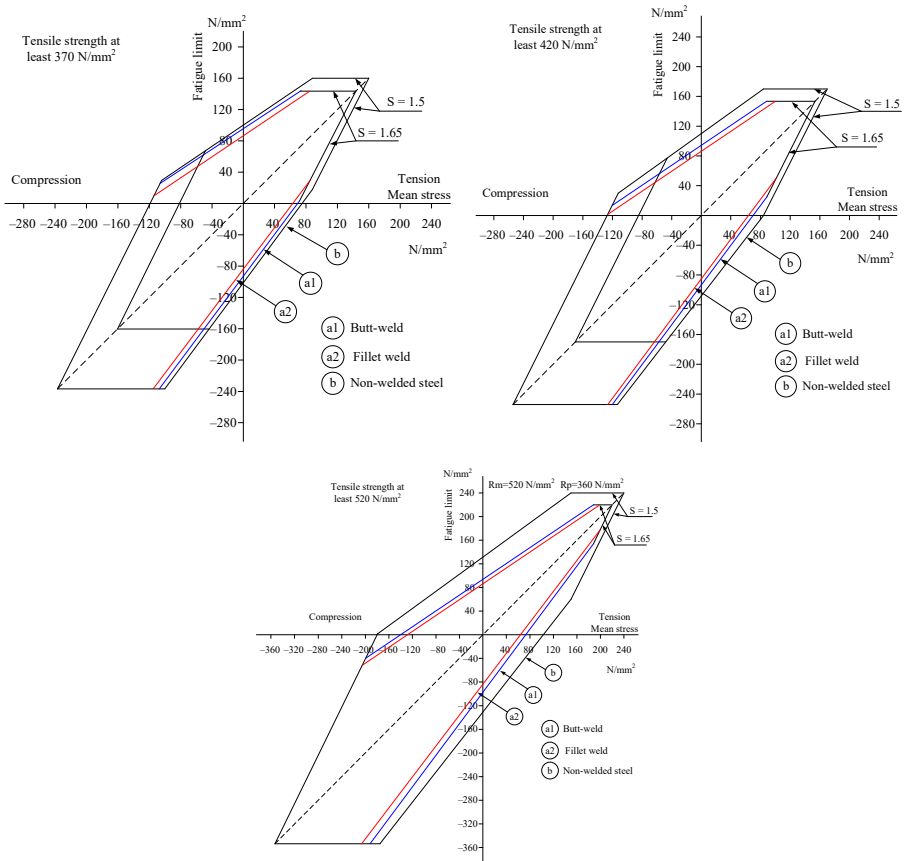


Figure 17. Goodman–Smith diagram of steel given in ERRI B 12/RP 17

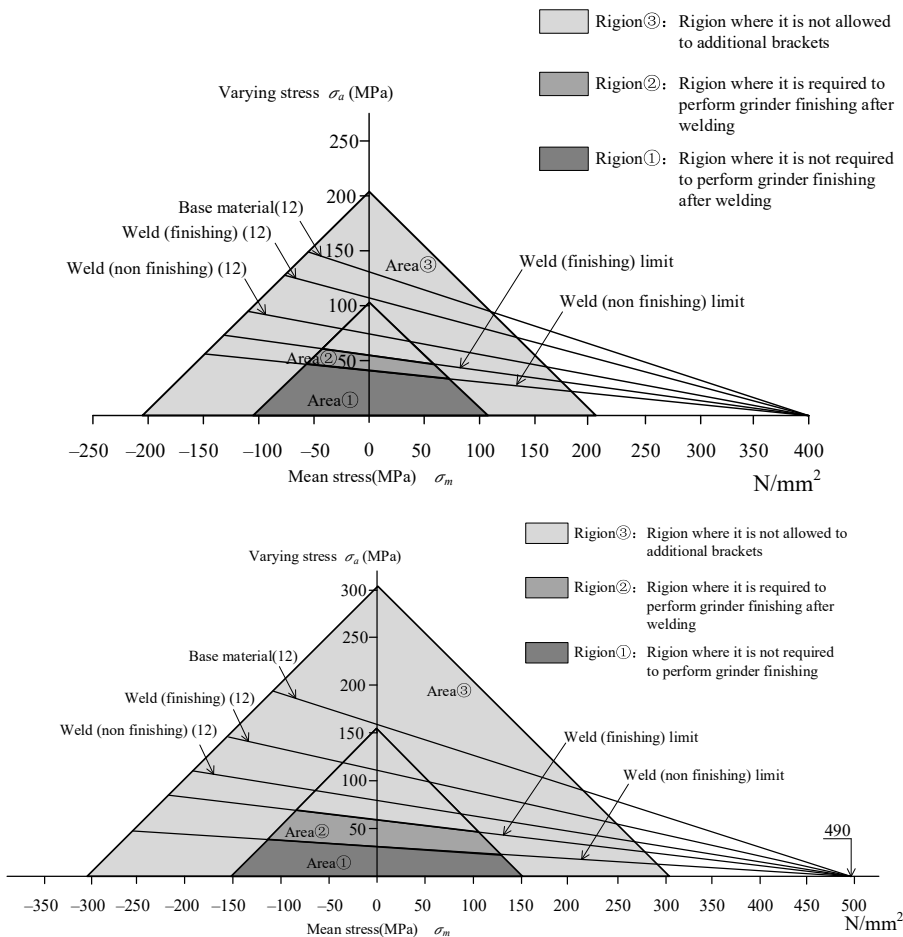
Source(s): Authors own work

520 N/mm². Three types of curves are used to specify the permissible stress for butt-weld, fillet weld and non-welded area, respectively. JIS E 4207 defined the Goodman–Haigh diagram, as shown in Figure 18. Three regions are taken into consideration to include the effects of weld grinding on the fatigue limit.

In the abovementioned Goodman diagram, the maximum- and minimum-stresses for all considered fatigue load cases have to be determined through the principal stress along the direction of maximum principal stress in the considered fatigue load cases. The amplitude- and mean-stress can be determined as:

$$\sigma_a = \frac{\sigma_{max} - \sigma_{min}}{2} ; \sigma_m = \frac{\sigma_{max} + \sigma_{min}}{2} \quad (2)$$

where σ_a is the amplitude of the stress cycle of considered fatigue load cases, σ_m is the mean stress for considered fatigue load cases, σ_{max} is the maximum principal stress for all considered fatigue load cases and σ_{min} is the minimum stress determined by resolving the



Source(s): Authors own work

Figure 18. Goodman–Haigh diagram given in JIS E4207

principal stress in the direction of maximum principal stress. Alternatively, DVS 1612 utilizes the normal stresses longitudinal and lateral to the seam direction (σ_{\parallel} and σ_{\perp}) and shearing stresses longitudinal to the seam direction (τ) to evaluate the fatigue strength through MKJ diagram, as shown in Figure 19. In the comparison of Goodman–Smith and Goodman–Haigh diagram, MKJ diagram gives a more detail description of the permissible stress depending upon the type of weld joint. In the assessment of fatigue, the concerned stress range has to lie in the envelope of the fatigue limit diagram in order to demonstrate the infinite life for the considered structure.

(2) Damage accumulative method

In the endurance strength method, the stress amplitude of cyclic loading has to be less than the fatigue limit defined by the fatigue strength diagram. Whereas in the operation, the service loading-induced stress could exceed the fatigue limit and then result in fatigue damage. Therefore, the fatigue damage assessment is usually conducted on the basis of the damage accumulation rule. A comprehensive review of time- and frequency-domain methods for fatigue damage estimation was given by Muñoz-Calvente *et al.* (2022). Fatigue damage estimation can be classified into two groups, including the time-domain methods and frequency-domain methods, as listed in Table 5. The first fatigue damage assessment method was proposed by Palmgren (1924) and Miner (1945) based on the ratio between the applied cycles and total cycles to failures, which considers the fatigue damage accumulative as a simple linear process and neglects the effects of the load-level and load-sequence and lack of load-interaction accountability. Accordingly, a huge number of investigations have been made to improve the Palmgren–Miner model, which results in several fatigue models, such as the double-linear model considering both crack initiation and propagation stages (Langer *et al.*, 1937), the nonlinear damage rules developed by Marco and Starkey (1954), energy damage models (including Leis, 1988 and Niu, Li, & Lee, 1987), continuum damage models (such as Chaboche & Lesne, 1988), as well as the probabilistic damage model proposed by Fernández-Canteli *et al.* (2014) and Fernández-Canteli (1982). A more detailed discussion of those models can be found in Fatemi and Yang (1998).

In the time-domain methods, the loading in terms of stress-time history observed in real operation conditions is needed to determine load cycles based on the rain flow counting method, which serves as basic input for fatigue damage assessment. However, due to economic and feasible reasons, the loading history with the limited time interval can be only obtained. This could be subjected to limitation when the load is a typical random because the limited load cycles cannot describe all load distributions in the service. For this reason, the

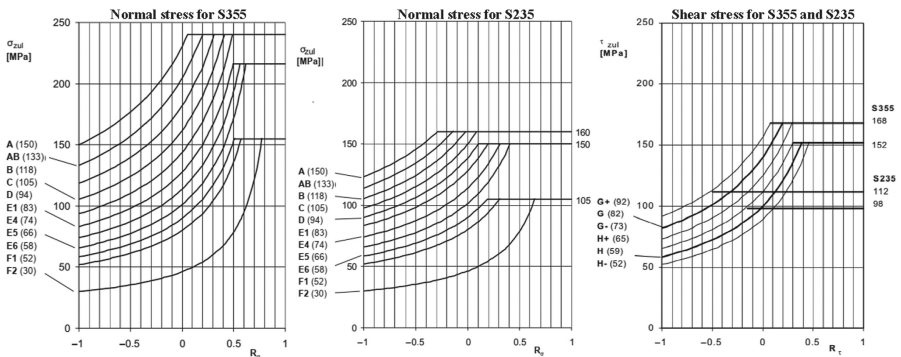


Figure 19. Permissible normal and shear stress for S355 and S235 given in DVS 1612

Source(s): Authors own work

Fatigue damage model		Expression
Time-domain	Palmgren–Miner	$D = \sum n_i / N_i$
	Marko–Starkey	$D = \sum (n_i / N_N)^{x_i}$
	Leis	$D = \frac{4\sigma_f'}{E} (2N_f)^{2b} + 4\sigma_f' e_f' (2N_f)^{b_1+c_1}$
	Niu	$D = (n/N)^{1/(a'+a)}$
	Fernández–Canteli	$p = 1 - \exp \left[- \left(\frac{(\log N - B)(\log \Delta \sigma - C) - \lambda}{\delta} \right)^\beta \right]$
Frequency-domain	Chaboche–Lesne	$D = 1 - [1 - (n/N)^{1/(1-a)}]^{1/(1+\beta)}$
	Narrow-band approximation	$\bar{D}^{NB} = v_0 C^{-1} (\sqrt{2m_0})^k \Gamma(1 + \frac{k}{2})$
	Range-mean approximation	$\bar{D}^{RC} = v_0 C^{-1} (\sqrt{2m_0} \alpha_2)^k \Gamma(1 + \frac{k}{2})$
	Wirsching–Light method	$\bar{D}_{RFC}^{WL} = [a(k) + [1 + a(k)](1 - e^{b(k)})] \bar{D}^{NB}$
	$\alpha_{0.75}$ method	$\bar{D}_{RFC}^{AL} = \alpha_{0.75}^2 \bar{D}^{NB}$
	Jiao–Moan method	$\bar{D}^{JM} = \rho_{JM} \bar{D}^{NB}$
	Gao–Moan method	$\bar{D}_{RFC}^{GM} = \bar{D}_P + \bar{D}_Q + \bar{D}_H$
	Dirlik method	$\bar{D}_{RFC}^{GM}(\sigma_a) = \frac{v_p}{C} \sigma_X^k \left[D_1 Q^k \Gamma(1+k) + (\sqrt{2})^k (1 + \frac{k}{2}) (D_2 R ^k + D_3) \right]$
	Zhao–Baker method	$\bar{D}_{RFC}^{ZB}(\sigma_a) = \frac{v_p}{C} \sigma_X^k \left[\omega a^{-\frac{k}{2}} \Gamma(1 + \frac{k}{2}) + (1 + \omega) 2^{\frac{k}{2}} \Gamma(1 + \frac{k}{2}) \right]$
	Tovo–Benasciutti method	$\bar{D}_{RFC}^{TB} = [b + (1-b)\alpha_2^{k-1}] \bar{D}^{NB}$
	Petrucci–Zucarello method	$\bar{D}_{RFC}^{PZ} = C^{-1} v_p \sqrt{m_0^k} e^{\Psi(a_1, a_2, b, \gamma)}$
	Zalaznik–Nagode method	$\bar{D}_{RFC}^{ZN} = v_p C_0(T)^{-1} \lambda_0^{k(T)/2} \left[D_1 Q^{k(T)} T(1+k(T)) + (\sqrt{2})^{k(T)} + \Gamma\left(1 + \frac{k(T)}{2}\right) (D_2 R ^{k(T)} + D_3) \right]$

Source(s): Palmieri *et al.* (2017)

Table 5. Fatigue damage estimation models for both time- and frequency-domains

frequency domain methods based on the statistical information of loading history are utilized to assessment the fatigue damage together with the S/N curve and Palmgren–Miner rule. In these methods, the random load histories are generally treated as a stationary Gaussian process, represented by the power spectral density (PSD). A random process can be characterized by the autocorrelation function $R_X(\tau)$, defined as follows:

$$R_X(\tau) = E[X(t)X(t + \tau)] \quad (3)$$

where $E[\cdot]$ operator is the probabilistic expected value. Similarly, this process can be expressed in the frequency domain with the two-sided PSD function, which is the Fourier transform of the autocorrelation function,

$$S_X(w) = \int_{-\infty}^{\infty} R_X(\tau) e^{-i w \tau} d\tau \quad (4)$$

The statistical information of spectral density $S_X(w)$ can be described through the means of the m th spectral moments λ_m :

$$\lambda_m = \int_{-\infty}^{\infty} w^m S_X(w) dw = (2\pi)^m \int_{-\infty}^{\infty} f^m S_X(f) df, m = 1, 2, \dots \quad (5)$$

The even moments correspond to the variance σ_X^2 of the random process X and its derivatives $\dot{X}(t)$ and $\ddot{X}(t)$:

$$\lambda_0 = \sigma_X^2, \lambda_2 = \sigma_{\dot{X}}^2, \lambda_4 = \sigma_{\ddot{X}}^2 \quad (6)$$

Based on the spectrum parameter, the expected peak occurrence frequency ν_0 and expected positive zero-crossing rate ν_p can be obtained as:

$$\nu_0 = \frac{1}{2\pi} \sqrt{\frac{\lambda_2}{\lambda_0}}, \nu_p = \frac{1}{2\pi} \sqrt{\frac{\lambda_4}{\lambda_2}} \quad (7)$$

These parameters are usually used to determine the total load cycles in the fatigue damage estimation for the frequency-domain methods. Additionally, the irregularity factor α_1, α_2 for the spectral density PSD can be expressed as:

$$\alpha_1 = \frac{\lambda_1}{\sqrt{\lambda_0 \lambda_2}}, \alpha_2 = \frac{\lambda_2}{\sqrt{\lambda_0 \lambda_4}} \quad (8)$$

where α_2 is the most commonly used parameter. When the random process tends to be a narrow-band process, the parameter α_2 is close to 1, otherwise, tends to zero. This parameter can be further employed to define the bandwidth parameter $\epsilon = \sqrt{1 - \alpha_2^2}$. When ϵ is close to 0, the signal tends to be a narrow band process, otherwise, the broadband process. Based on the derivation of above-mentioned spectral parameters, the distribution of rainflow cycle can be obtained, which is considered the main difference compared to time-domain methods. Rice (1944) established the probability density function (PDF) of the peak amplitude for a general broadband process $X(t)$:

$$P_p(x) = \frac{\sqrt{1 - \alpha_2^2}}{\sqrt{2\pi}\sigma_x} e^{-\frac{x^2}{2\sigma_x^2(1 - \alpha_2^2)}} + \frac{\alpha_2 x}{\sigma_x^2} e^{-\frac{x^2}{2\sigma_x^2}} \Phi\left(\frac{\alpha_2 x}{\sigma_x \sqrt{1 - \alpha_2^2}}\right) \quad (9)$$

where $\Phi(\cdot)$ is the standard normal cumulative distribution function:

$$\Phi(z) = \frac{1}{\sqrt{2\pi}} \int_{-\infty}^z e^{-\frac{t^2}{2}} dt \quad (10)$$

Based on the S–N curve, the relationship between the stress and fatigue life is

$$S^k N = C \quad (11)$$

where N is the number of cycles to failure at the stress amplitude S , C and k are the fatigue–strength coefficient and fatigue–strength exponent, respectively. In the time-domain method, S is usually determined through rainflow counting method and is considered a deterministic parameter. Whereas, for a random process, the stress cycle amplitudes are non-deterministic parameters, which are calculated through the PDF $p(S_i)$. The number of cycles n_i for stress range $(S_i, S_i + \Delta S)$ in the time period T can be determined as:

$$n_i = v_p T p(S_i) \Delta S \quad (12)$$

Therefore, based on the Palmgren–Miner method, the fatigue damage can be expressed as:

$$D = \sum D_i = \sum \frac{n_i}{N_i} = \sum \frac{v_p T p(S_i) \Delta S}{N_i} = v T \int_0^\infty \frac{p(S_i)}{N(S_i)} dS \quad (13)$$

$$D = \frac{v_p T}{C} \int_0^\infty S^k p(S) dS \quad (14)$$

and the damage per unit time thus can be defined as:

$$d = \frac{D}{T} = \frac{v_p}{C} \int_0^\infty S^k p(S) dS \quad (15)$$

It can be seen that the main work for frequency-domain method is to formulate a PDF for stress–cycle amplitude distribution. Therefore, huge works have been made to develop the rainflow PDF approximation methods, as listed in Table 6. The pioneering work was conducted by Dirlík (1985) modelling the rainflow PDF through combining one exponential and two Rayleigh probability densities. Zhao and Baker (1992) proposed a rainflow PDF through the linear combination of the Weibull and Rayleigh PDF. Based on the Rayleigh, a standard Rayleigh and a half-Gaussian distribution, Park, Choung, and Kim (2014) developed another rainflow PDF. Similarly, Jun and Park (2020) further corrected the rainflow PDF through a Rayleigh, a standard Rayleigh, a half-Gaussian and an additional exponential distribution.

Apart from the rainflow PDF approximation methods, the narrowband formulation together with the narrowband correction factor is also used to estimate the fatigue damage for a broadband random process, such as Wirsching–Light method (Wirsching & Light, 1980), Ortiz–Chen method (Ortiz & Chen, 1987) and Tovo–Benasciutti method (Tovo *et al.*, 2002). To deal with the multimodal in the broadband process, a spectral density is usually considered as a superposition of two or more narrowband processes, and then each narrowband process-induced damage is estimated by the related approximation method, such as Jiao–Moan method (Jiao & Moan, 1990), Sakai–Okamura method (Sakai & Okamura, 1995), Fu–Cebon method (Fu & Cebon, 2000), Low method (Low, 2014) and Gao–Moan

Models	Expressions
Narrow band (Miles <i>et al.</i> , 1954)	$p_a(s) = \frac{s^{-2}}{\sigma_s^2} e^{-2s/\sigma_s}$
Dirlík method (Dirlík, 1985)	$p_a(z) = \frac{1}{\sqrt{\pi} \omega_0} \left(\frac{G_1}{Q} e^{-z/Q} + \frac{G_2 Z}{R^2} e^{-z/R^2} + G_3 Z e^{-z/2} \right)$
Zhao and Baker method (Zhao & Baker, 1992)	$p_a(z) = \omega \alpha \beta Z^{\beta-1} e^{-\alpha Z^\beta} + (1 - \omega) Z e^{-z/2}$
Park method (Part <i>et al.</i> , 2014)	$p_a(z) = c_{R1} \frac{z}{\sigma_{R1}^2} e^{-z/\sigma_{R1}^2} + c_{R2} Z e^{-z/2} + c_G \frac{2}{\sqrt{2\pi} \sigma_G} e^{-\frac{z^2}{2\sigma_G^2}}$
Jun–Park (Jun & Park, 2020)	$p_a(z) = Q_c \left[D_1 \frac{1}{\sigma_E} e^{-z/E} + D_2 \frac{z}{\sigma_R^2} e^{-z/\sigma_R^2} + D_3 Z e^{-z/2} + D_4 \frac{2}{\sqrt{2\pi} \sigma_H} e^{-\frac{z^2}{2\sigma_H^2}} \right]$

Source(s): Authors own work

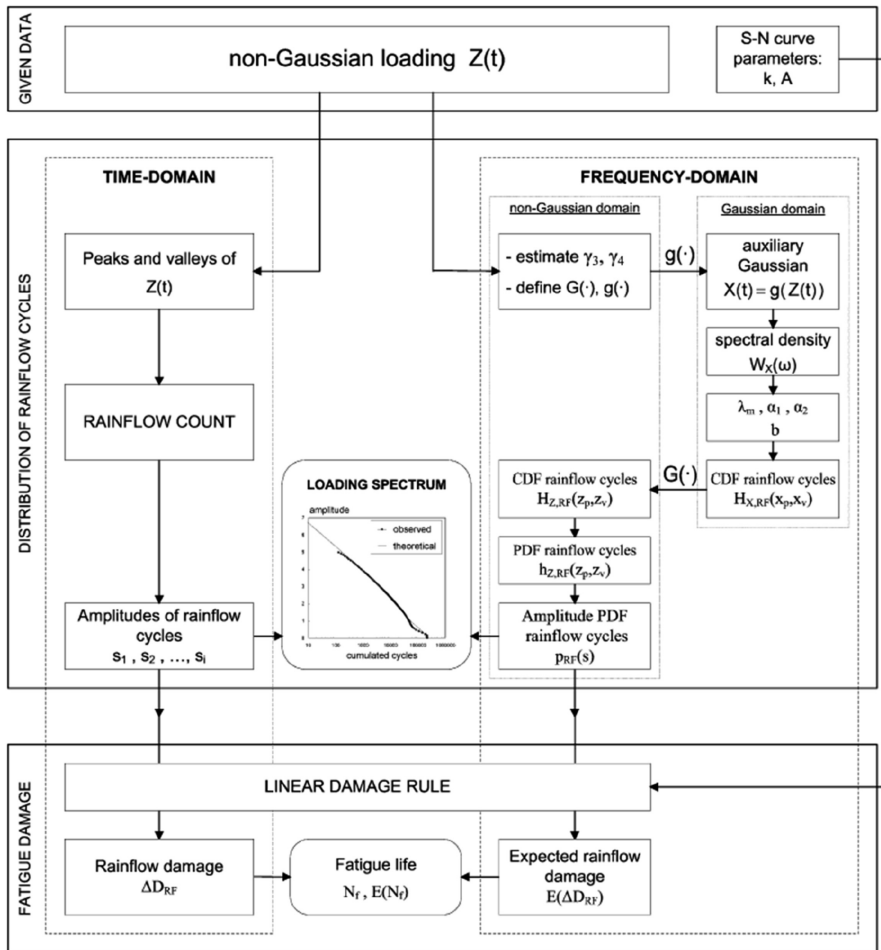
Table 6.
Rainflow cycle PDF
approximation
methods

method (Gao & Moan, 2008). Alternatively, some other researchers directly used the narrow band formulation to estimate fatigue damage for each narrow band process and studied the combination methods for individual damage obtained, such as the Lotsberg method (Lotsberg, 2005), Huang–Moan method (Huang & Moan, 2006), Han–Ma (Han, Ma, Qu, Yang, & Qin, 2016) and Bands method (Braccesi, Cianetti, & Tomassini, 2015). Considering 104 different PSD spectra and three different fatigue–strength exponents, Ales Zorman, Slavič, and Boltezar (2023) compared the frequency-domain methods to the time-domain method using the numerical simulation and concluded that Ortiz–Chen, $\alpha_{0.75}$, Tovo–Benasciutti 2, Dirlik, Park and Jun–Park methods can give an acceptable engineering accuracy for small values of the $S-N$ curve slope ($k=3.324$). For a larger fatigue strength exponent ($k=7.3$), Ortiz–Chen, $\alpha_{0.75}$, Park, Jun–Park and Huang–Moan methods can yield a relatively smaller error below 25%. Table 1 lists the most cited frequency–domain-based fatigue damage models. Dirlik and Benasciutti (2021) performed a comprehensive review of the spectral methods, especially focusing on the review of comparison investigations for spectral methods, and concluded that Dirlik and TB methods generally give a better estimation.

The aforementioned spectral methods invariably treated the random vibration as a stationary Gaussian process. However, due to local irregularities on the track, the vibration in railway vehicle usually expresses non-stationary and non-Gaussian characteristics. A number of scholars investigated how the non-stationary and non-Gaussian affect the vibration fatigue. Rizzi, Przekop, and Turner (2011) and Kihm, Rizzi, Ferguson, and Halfpenny (2013) pointed out that for a stationary excitation the non-Gaussian signal results in a Gaussian stress response, and the non-stationarity is the origin of non-Gaussian response. Through studying the vibration fatigue life of Y-shaped specimens considering the non-Gaussianity and non-stationarity loading, Palmieri, Česnik, Slavič, Cianetti, and Boltezar (2017) concluded that the Gaussian theoretical-based methods could be questionable when the excitation is non-stationary and non-Gaussian excitation, and the fatigue life was found to be significantly impacted due to characteristics of non-Gaussianity and non-stationarity in the vibration loading. Capponi, Česnik, Slavič, Cianetti, and Boltezar (2017) defined an index to quantify the non-stationarity of a signal and investigated the effects of non-stationary on fatigue life. The obtained results further show that the non-stationary can have significantly shorter fatigue life compared with those caused by stationary excitations.

To assess the fatigue damage arising from the non-Gaussian loading, the Gaussian-based methods were further modified. Benasciutti and Tovo (2006) utilized a nonlinear transformation to transform the Gaussian load to a non-Gaussian load and further proposed the non-Gaussian-based frequency domain method for the narrow-band approximation and TB method, as shown in Figure 20. Wolfsteiner (2017) proposed a new methodology to estimate fatigue damage of non-stationary random vibration through the decomposition of a non-stationary vibration signal into several stationary vibrations with Gaussian distributions. The essential of this method is to estimate the distribution of statistical moments over the frequency band of the given non-stationary signal. This method was further employed to assess the fatigue damage of rail guard (Wolfsteiner & Breuer, 2013). Jiang *et al.* investigated on the non-Gaussian random vibration fatigue analysis and accelerated test (Jiang, Tao, & Chen, 2021).

In both time- and frequency-domain methods, the $S-N$ curve is the essential part of the fatigue damage estimation, which defines the relationship between the stress range and the number of cycles to failure. This relationship is subjected to variations considering different materials and weld joint details. Therefore, a huge number of tests have been performed to establish the $S-N$ curve for the interested material or design detail. The mathematical expression of $S-N$ curves can be classified into deterministic models and probabilistic models. Castillo and Fernández–Canteli summarize the typical $S-N$ curve models (Castillo & Fernández-Canteli, 2009), as listed in Table 7. In most industrial standards, the $S-N$ curve is



Source(s): Benasciutti and Tovo (2006)

Figure 20. The non-Gaussian TB method together with the time domain method for the case of a non-Gaussian loading

represented by the Basquin equation (OH, 1910), such as IIW standard, BS7608, JIS 4207, and Eurocode 3. Figure 21 illustrates the typical S–N curves defined in the IIW, BS7608, Eurocode 3 and JIS 4207. It can be seen that the S/N curves given by different standards are subjected to huge deviations, which gives a big challenge to select the right S/N curve based on the design detail. Therefore, Dong *et al.* proposed the structural stress-based master S/N curve in terms of the structure stress rather than the nominal stress (Dong, 2021).

5. Research gaps and discussions

The above-mentioned investigations invariably suggest that the main driving force for the vibration fatigue of railway bogie is the short-pitch irregularities-induced high frequency vibration. Whereas the current design method is still based on the quasi-static method and neglects the high frequency vibration-induced mode resonance in the structure. The methodologies used to assess the fatigue damage of structure could be considered as a

Table 7.
Typical S–N curve
models

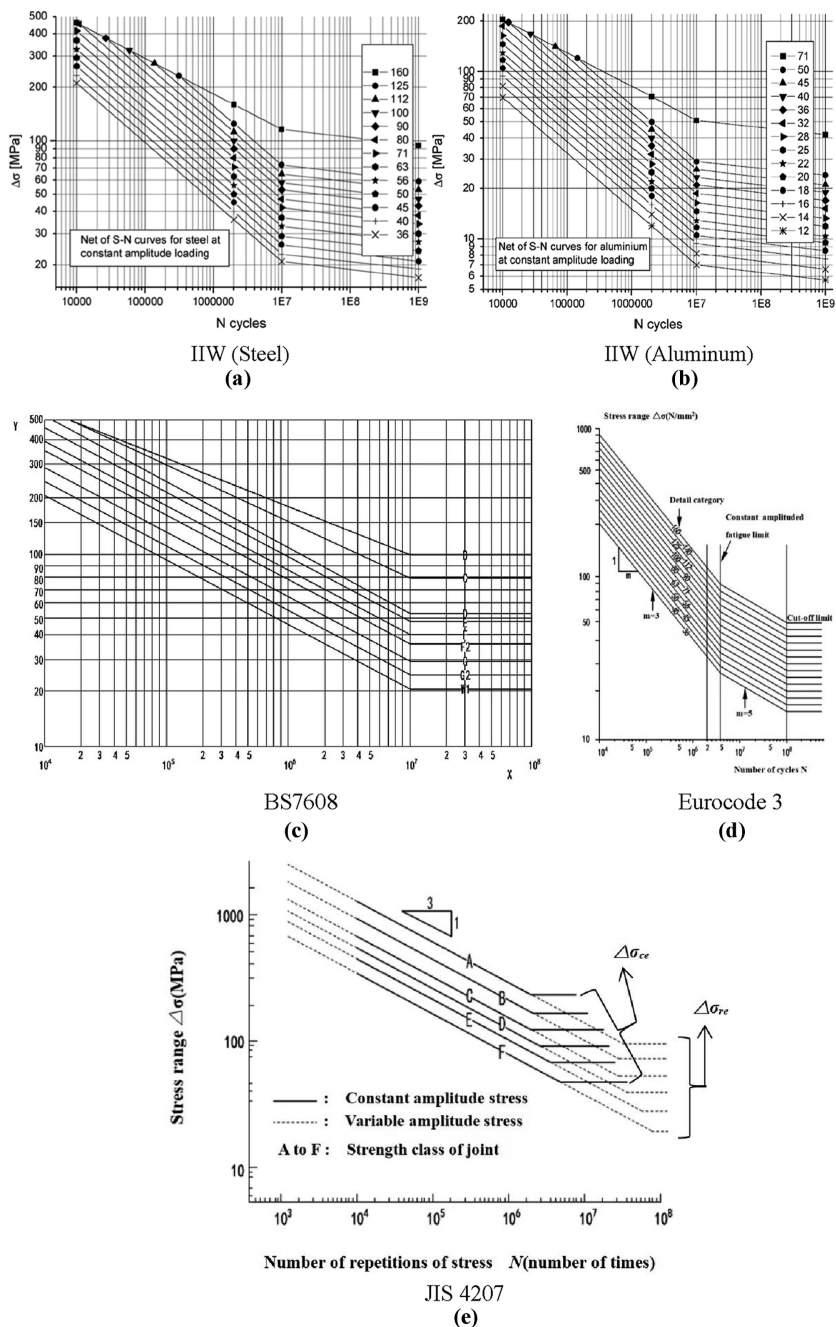
Model	Expression
Basquin	$\log N = A - B \log \Delta\sigma$
Stromeyer	$\log N = A - B \log(\Delta\sigma - \Delta\sigma_0)$
Palmgren	$\log(N + D) = A - B \log(\Delta\sigma - \Delta\sigma_0)$
Weibull	$\log(N + D) = A - B \log((\Delta\sigma - \Delta\sigma_0)/(\Delta\sigma_{st} - \Delta\sigma))$
Stüssi	$\log N = A - B \log((\Delta\sigma - \Delta\sigma_0)/(\Delta\sigma_{st} - \Delta\sigma))$
Bastenaire	$(\log N - B)((\Delta\sigma - \Delta\sigma_0)) = A \exp[-C((\Delta\sigma - \Delta\sigma_0))]$
Spindel–Haibach	$\log\left(\frac{N}{N_0}\right) = A \log(\Delta\sigma/\Delta\sigma_0) - B \log(\Delta\sigma/\Delta\sigma_0) +$ $+ B\{(1/\alpha)\log[1 + (\Delta\sigma/\Delta\sigma_0)^{-2\alpha}]\}$
Castillo–Canteli	$\log(N/N_0) = \frac{\lambda + (-\log(1-p))^\beta}{\log(\Delta\sigma/\Delta\sigma_0)}$
Kohout–Vechet	$\log\left(\frac{\Delta\sigma}{\Delta\sigma_\infty}\right) = \log\left(\frac{N+N_1}{N+N_1}\right)^b$
Pascual–Meeker	$\log N = A - B \log(\Delta\sigma - \Delta\sigma_0)$

Source(s): Castillo and Fernández-Canteli (2009)

postprocess procedure for dynamic stress and focus on improving the assessment accuracy of fatigue damage for a given loading condition. The system dynamics and the fatigue strength assessment are not coupled and are considered as separated fields. It is known that the loading of fatigue strength assessment is the dynamic response of system dynamics. Therefore, the core of improving the survival probability of vibration fatigue is to develop a systematic design method coupling the strength of structure and the system dynamics of the vehicle and track system, so as to achieve a reasonable matching relationship between the considered components and the service boundary conditions.

5.1 Systematic design methodologies for the vibration fatigue

A systematic design methodology is needed to account for the contribution of mode vibration of structure through coupling the system dynamics and the strength on the basis of tradition design and verification methods. Figure 22 illustrates a suggested design flowchart for the vibration fatigue. In the quasi-static design phase, the traditional static and fatigue strength analyses are conducted based on the loads given in the standard, such as EN 13749, UIC 515–4/615–4 and JIS 4207/4208. This phase is used to demonstrate the satisfaction of current design codes based on the simulation of the FE model of interested component, which neglects the real operating conditions. Therefore, a dynamic design phase is suggested to consider the typical vibration conditions, in which a vibration spectrum obtained through either field tests or numerical simulations is considered as an input for a vibration model. This vibration model could be a single component or the whole vehicle neglecting the wheel/rail contact based on the finite element method or rigid/flexible coupled theory. The identified weak point is considered as the dynamic weak point since the contribution of mode vibration is taken into consideration which could lead to different weak points. The weak points identified in both quasi-static and dynamic phases should be treated carefully for the design of vibration fatigue. Another important aspect of this phase is to evaluate the contribution of vibration mode based on the typical vibration spectrum, where the critical geometry parameters could be adjusted to achieve a reasonable modal matching from the vibration and fatigue damage point of view. In the third phase, a more comprehensive model of vehicle/track coupled dynamics based on the rigid/flexible coupling theory is needed to simulate all possible service conditions for rail vehicle, so as to obtain the characteristic load spectrum of



Source(s): Authors own work

Figure 21. S-N curves defined in IIW, BS7608, Eurocode 3, and JIS 4207

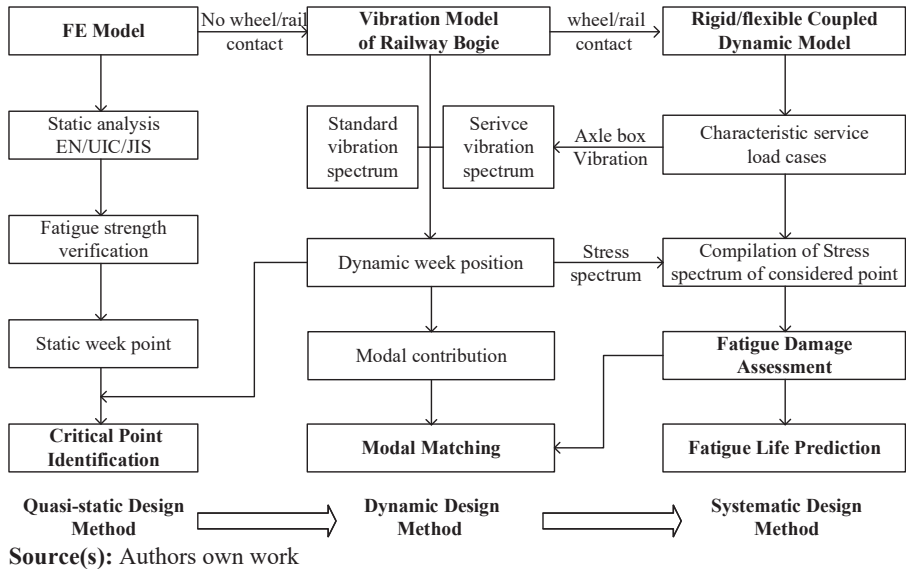


Figure 22.
A systematic design method for vibration fatigue of railway vehicle

the considered region. This can further facilitate the compilation of the stress spectrum of interested points, thereby the fatigue damage estimation and fatigue life prediction. To obtain a reasonable estimation, the S/N curve and fatigue damage should be selected carefully and the degradation process of loading and material properties also should be taken into consideration. This framework aims to integrate the system dynamics into the strength design of interested components so as to consider the contribution of vibration mode, which is expected to improve the survival probability of vibration fatigue.

5.2 Characterization of typical vibration spectrum of wheel/rail for railway bogie

The design of vibration fatigue should be based on the understanding of typical loads arising from coupling subsystems of railway bogie, including the wheel/rail interaction, traction and braking and aerodynamics, as well as loads from the car body. The wheel/rail interaction serves as the basic input for rail vehicles, it is thus desirable to determine the features of coupled vibration of wheel/rail considering different track properties. The dominating frequency bands, including P2 force and other dominating frequencies contributing to the formation of rail corrugation and wheel polygonal wear, should be treated carefully in the modal matching. Wu *et al.* summarized the typical wheel/rail coupled vibration modes of rail vehicles in the vertical direction (Wu *et al.*, 2023), whereas the coupled vibration modes in the lateral direction are still needed to be further clarified. The axle box vibration spectrum could be taken as a representative of wheel/rail coupled vibration, and a database for characteristic vibration spectrums of axle box is thus suggested on the basis of field test measurements. This could be considered as an input for the random vibration model of railway bogie in the dynamic design phase. Regarding traction and braking-induced loads, the effects of mechanical–electrical coupled loads on railway bogie should be taken into consideration, especially for the high frequency component. For the thin-shell structure in rail vehicle, the fluid–solid coupling-induced dynamic loads should be taken into consideration through either simulation of a fluid–solid coupled dynamic model or field tests.

5.3 Systematic modal matching between the railway bogie and track system

Modal matching is the core of avoiding the vibration fatigue of railway bogie arising from the wheel/rail high frequency vibration. Theoretically, the natural frequencies of railway bogie should avoid typical dominating frequency bands of wheel/rail interaction. Whereas the principle for determination of the difference between the nature frequency and the excitation frequency still remains in question. In the mechanical vibration, the natural frequency of the system is suggested to stay away from the frequency range of bandwidth of dominating frequency. This could be still a big challenge for railway bogie design since the railway bogie is characterized by multi-modes. The natural frequencies of bogie frame cannot completely avoid all possible exciting frequencies, which mean that the railway bogie has to withstand the impacts due to the modal vibration arising from external excitations. A sophisticated modal matching criterion is thus needed to achieve the reasonable matching between the railway bogie and the coupling boundary.

5.4 Fatigue damage assessment for full life cycle of railway bogie

The fatigue damage assessment for railway bogie still shows deviations with respect to the real operation conditions, although huge efforts have been made. For vibration fatigue, the failure of interested components usually failed due to the structural resonance at a relatively high frequency range. Whereas the definition of S/N curve in the current standard neglects the influence of loading frequency and few of investigations address the frequency effects of S/N curve for railway bogie material. Although a number of fatigue damage assessment models have been developed based on different considerations, the linear Palmgren–Miner model is still a widely used model in the application due to the features of simplicity and convenient. For the frequency domain method, a well-validated model should be established to deal with the non-Gaussian and non-stationary signal in the railway. The load spectrum definition is essential for fatigue damage assessment. In the railway, the wheel/rail interaction is subjected to a degradation process due to the formation of uneven wear on the wheel and railhead surfaces, thereby the evolution of loading for railway bogie. For the full life cycle fatigue damage assessment, the degradation process in the load spectrum has to be addressed in the load definition, especially the evolution process arising from wheel OOR. In addition, it is suggested that the fatigue mechanism and damage mechanism under resonance conditions should be further studied and expounded, which could facilitate to improve the structural design so as to reduce the structural resonance-induced fatigue failure.

5.5 Mitigation of wheel/rail high frequency vibration

The vibration fatigue of railway bogie is mainly caused by the wheel/rail high frequency vibration. It is thus desirable to study methodologies to reduce the wheel/rail high frequency vibration-induced impacts, such as suppression of formation of wheel polygonal wear and rail corrugation, a reasonable limit value for the short-pitch irregularities and vibration reduction for high frequency vibration transmission.

6. Conclusions

The vibration fatigue of railway bogie has been considered the main concern of railway operators due to its highly adverse influences. This paper deals with the wheel/rail high frequency vibration-induced vibration fatigue in the railway bogie, mainly focusing on the characteristics of wheel/rail high frequency vibration, high frequency vibration-induced vibration fatigue failures in railway bogie, and the methodologies used to assess the vibration fatigue-induced fatigue damage, then the research gaps have been further discussed. This review is expected to explore the vibration fatigue of railway bogie and facilitate the development of the forward design methodology of vibration fatigue for railway bogie.

References

- An, Q., Li, F., Huang, Y., Fu, M., & Yu, C. (2009). Fatigue strength assessment for bogie welded frame based on JIS standard. *Electric Drive for Locomotives*, 04, 26–29.
- Angeli, A., Cornelis, B., & Troncosi, M. (2016). Fatigue damage spectrum calculation in a mission synthesis procedure for sine-on-random excitations. *Journal Physics: Conference Series*, 744(1), 012089. doi: [10.1088/1742-6596/744/1/012089](https://doi.org/10.1088/1742-6596/744/1/012089).
- Benasciutti, D., & Tovo, R. (2006). Fatigue life assessment in non-Gaussian random loadings. *International Journal of Fatigue*, 28(7), 733–746. doi: [10.1016/j.ijfatigue.2005.09.006](https://doi.org/10.1016/j.ijfatigue.2005.09.006).
- Bethel, L., Chen, G., Wang, P., Xu, J., Cheng, J., & Fang, J. (2022). Random vibration analysis of tram-track interaction on a curve due to the polygonal wheel and track irregularity. *Vehicle System Dynamics*, 60(4), 1125–1147. doi: [10.1080/00423114.2020.1847299](https://doi.org/10.1080/00423114.2020.1847299).
- Braccesi, C., Cianetti, F., & Tomassini (2015). A new frequency domain criterion for the damage evaluation of mechanical components. *International Journal of Fatigue*, 70, 417–427. doi: [10.1016/j.ijfatigue.2014.07.005](https://doi.org/10.1016/j.ijfatigue.2014.07.005).
- Cai, W., Chi, M., Tao, G., Wu, X., & Wen, Z. (2019). Experimental and numerical investigation into formation of metro wheel polygonalization. *Shock and Vibration*, 2019, 1538273. doi: [10.1155/2019/1538273](https://doi.org/10.1155/2019/1538273).
- Cai, W., Chi, M., Wu, X., Sun, J., Zhou, Y., Wen, Z., & Liang, S. (2020). A long-term tracking test of high-speed train with wheel polygonal wear. *Vehicle System Dynamics*, 59(11), 1735–1758. doi: [10.1080/00423114.2020.1786592](https://doi.org/10.1080/00423114.2020.1786592).
- Cai, W., Chi, M., Wu, X., Sun, J., Zhou, Y., Wen, Z., & Liang, S. (2021). A long-term tracking test of high-speed train with wheel polygonal wear. *Vehicle System Dynamics*, 59(11), 1735–1758. doi: [10.1080/00423114.2020.1786592](https://doi.org/10.1080/00423114.2020.1786592).
- Cai, W., Wu, X., Chi, M., Yang, C., & Huang, H. (2022). Wheel polygonisation growth due to multiple wheelsets/track coupling vibration. *Vehicle System Dynamics*, 61(1), 77–199. doi: [10.1080/00423114.2022.2045028](https://doi.org/10.1080/00423114.2022.2045028).
- Cai, W., Chi, M., Wu, X., Yang, N., & Huang, H. (2023). Effect of wheel initial state on the growth of polygonal wear on high-speed trains. *Wear*, 526, 204894. doi: [10.1016/j.wear.2023.204894](https://doi.org/10.1016/j.wear.2023.204894).
- Capponi, L., Česnik, M., Slavič, J., Cianetti, F., & Boltezar, M. (2017). Non-stationarity index in vibration fatigue: Theoretical and experimental research. *International Journal of Fatigue*, 104, 221–230. doi: [10.1016/j.ijfatigue.2017.07.020](https://doi.org/10.1016/j.ijfatigue.2017.07.020).
- Carson, R., & Johnson, K. (1971). Surface corrugations spontaneously generated in a rolling contact disc machine. *Wear*, 17(1), 59–72. doi: [10.1016/0043-1648\(71\)90014-7](https://doi.org/10.1016/0043-1648(71)90014-7).
- Castillo, E., & Fernández-Canteli, A. (2009). *A unified statistical methodology for modeling fatigue damage*. Springer Science & Business Media, Berlin.
- Chaboche, J., & Lesne, P. (1988). A non-linear continuous fatigue damage model. *Fatigue and Fracture of Engineering Materials & Structures*, 11(1), 1–7. doi: [10.1111/j.1460-2695.1988.tb01216.x](https://doi.org/10.1111/j.1460-2695.1988.tb01216.x).
- Chang, C., Cai, Y., Chen, B., Li, Q., & Lin, P. (2022). Experimental study of the wheel/rail impact caused by wheel flat within 400 km/h using full-scale roller rig. *Railway Sciences*, 1, 76–89. doi: [10.1108/rs-04-2022-0018](https://doi.org/10.1108/rs-04-2022-0018).
- Chen, G., Zhang, S., Wu, B., Zhao, X., Wen, Z., Quyang, H., & Zhu, M. (2020). Field measurement and model prediction of rail corrugation. *Proceedings of the Institution of Mechanical Engineers, Part F: Journal of Rail and Rapid Transit*, 234(4), 381–392. doi: [10.1177/0954409719877318](https://doi.org/10.1177/0954409719877318).
- Chen, Z., Zhi, Y., Wang, K., & Zhai, W. (2023). Effect of drive and transmission system on wheel polygonal wear of an heavy-haul locomotive. *Vehicle System Dynamics*, 61(12), 3047–3066. doi: [10.1080/00423114.2022.2153066](https://doi.org/10.1080/00423114.2022.2153066).
- Clark, R., Scott, G., & Poole, W. (1988). Short wave corrugations-an explanation based on stick-slip vibrations. *Proceedings of Applied Mechanics Rail Transportation Symposium* (Vol. 96, pp. 141–148). Washington.

- Daniel, W., Horwood, R., Meehan, P., & Wheatley, N. (2008). Analysis of rail corrugation in cornering. *Wear*, 265(9-10), 1183–1192. doi: [10.1016/j.wear.2008.02.030](https://doi.org/10.1016/j.wear.2008.02.030).
- Deng, C. (2019). Spectral induction method of vibration in rail vehicles' measurement environment. *Journal of Tongji University (Natural Science)*, 47(10), 1514–1519.
- Ding, J., Zhang, P., & Wang, P. (2016). Analysis of vibration test standard and field measurement data for rolling stock equipment. *Journal of Mechanical Engineering*, 52(22), 129. doi: [10.3901/jme.2016.22.129](https://doi.org/10.3901/jme.2016.22.129).
- Dirlik, T. (1985). *Application of computers in fatigue analysis*. University of Warwick, Coventry.
- Dirlik, T., & Benasciutti, D. (2021). Dirlik and tovo-benasciutti spectral methods in vibration fatigue: A review with a historical perspective. *Metals*, 11(9), 1333. doi: [10.3390/met11091333](https://doi.org/10.3390/met11091333).
- Dong, P. (2021). A structural stress definition and numerical implementation for fatigue analysis of welded joints. *International Journal of Fatigue*, 23(10), 865–876. doi: [10.1016/s0142-1123\(01\)00055-x](https://doi.org/10.1016/s0142-1123(01)00055-x).
- Dong, Z., Wang, W., Dai, S., & Li, G. (2023). Research on vibration fatigue and failure mechanism of the wire bracket for high-speed train. *Engineering Failure Analysis*, 151, 107409. doi: [10.1016/j.engfailanal.2023.107409](https://doi.org/10.1016/j.engfailanal.2023.107409).
- Fatemi, A., & Yang, L. (1998). Cumulative fatigue damage and life prediction theories: A survey of the state of the art for homogeneous materials. *International Journal of Fatigue*, 20(1), 9–34. doi: [10.1016/s0142-1123\(97\)00081-9](https://doi.org/10.1016/s0142-1123(97)00081-9).
- Feng, Y., Qu, S., Li, F., Dai, H., & Shu, K. (2023). Nonlinear vibration of the axle box front cover of high-speed train and its effect on connecting bolts. *Engineering Failure Analysis*, 143, 106912. doi: [10.1016/j.engfailanal.2022.106912](https://doi.org/10.1016/j.engfailanal.2022.106912).
- Fernández-Canteli, A. (1982). *Statistical interpretation of the Miner-number using an index of probability of total damage*. Birkhauser Verlag AG.
- Fernández-Canteli, A., Blasón, S., Correia, J., & Jesus, A. (2014). A probabilistic interpretation of the Miner number for fatigue life prediction. *Frattura ed Integrità Strutturale*, 8(30), 327–339. doi: [10.3221/igf-esis.30.40](https://doi.org/10.3221/igf-esis.30.40).
- Fourie, D., Frohling, R., & Heyns, S. (2020). Railhead corrugation resulting from mode-coupling instability in the presence of veering modes. *Tribology International*, 152(1), 106499. doi: [10.1016/j.triboint.2020.106499](https://doi.org/10.1016/j.triboint.2020.106499).
- Fu, T., & Cebon, D. (2000). Predicting fatigue lives for bi-modal stress spectral densities. *International Journal of Fatigue*, 22(1), 11–21. doi: [10.1016/s0142-1123\(99\)00113-9](https://doi.org/10.1016/s0142-1123(99)00113-9).
- Gao, Z., & Moan, T. (2008). Frequency-domain fatigue analysis of wide-band stationary Gaussian processes using a trimodal spectral formulation. *International Journal of Fatigue*, 30(10-11), 1944–1955. doi: [10.1016/j.ijfatigue.2008.01.008](https://doi.org/10.1016/j.ijfatigue.2008.01.008).
- Grassie, S. (2009). Rail corrugation: Characteristics, causes, and treatments. *Proceedings of the Institution of Mechanical Engineers, Part F: Journal of Rail and Rapid Transit*, 223(6), 581–596. doi: [10.1243/09544097jrrt264](https://doi.org/10.1243/09544097jrrt264).
- Han, X. (2021). Vehicle vibration analysis based on spectrum induction. *Noise and Vibration Control*, 41(5), 26–30.
- Han, C., Ma, Y., Qu, X., Yang, M., & Qin, P. (2016). A practical method for combination of fatigue damage subjected to low-frequency and high-frequency Gaussian random processes. *Applied Ocean Research*, 60, 47–60. doi: [10.1016/j.apor.2016.08.007](https://doi.org/10.1016/j.apor.2016.08.007).
- Himmelblau, H., Piersol, A., Wise, J., & Grundvig, M. (1994). Handbook for dynamic data acquisition and analysis. In *IES Recommended Practice*. Institute of Environmental Sciences.
- Hu, W., Liu, Z., Liu, D., & Hai, X. (2017). Fatigue failure analysis of high speed train gearbox housings. *Engineering Failure Analysis*, 73, 57–71. doi: [10.1016/j.engfailanal.2016.12.008](https://doi.org/10.1016/j.engfailanal.2016.12.008).
- Huang, W., & Moan, T. (2006). Fatigue under combined high and low frequency loads. In *25th International Conference on Offshore Mechanics and Arctic Engineering*, Hamburg. ASME, Paper No. OMAE2006-92247.

- Iwnicki, S., Nielsen, J., & Tao, G. (2023). Out-of-round railway wheels and oligonization. *Vehicle System Dynamics*, 61(7), 1787–1830. doi: [10.1080/00423114.2023.2194544](https://doi.org/10.1080/00423114.2023.2194544).
- Jiang, Y., Tao, J., & Chen, X. (2021). *Non-Gaussian random vibration fatigue analysis and accelerated test*. Singapore: Springer Singapore.
- Jiao, G., & Moan, T. (1990). Probabilistic analysis of fatigue due to Gaussian load processes. *Probabilistic Engineering Mechanics*, 5(2), 76–83. doi: [10.1016/0266-8920\(90\)90010-h](https://doi.org/10.1016/0266-8920(90)90010-h).
- Jin, X., Wen, Z., Wang, K., Zhou, Z., & Liu, Q. (2006). Three-dimensional train-track model for study of rail corrugation. *Journal of Sound and Vibration*, 293(3-5), 830–855. doi: [10.1016/j.jsv.2005.12.013](https://doi.org/10.1016/j.jsv.2005.12.013).
- Jin, X., Wu, L., Fang, J., Zhong, S., & Ling, L. (2012). An investigation into the mechanism of the polygonal wear of metro train wheels and its effect on the dynamic behaviour of a wheel/rail system. *Vehicle System Dynamics*, 50(12), 1817–1834. doi: [10.1080/00423114.2012.695022](https://doi.org/10.1080/00423114.2012.695022).
- Jin, X., Li, X., Li, W., & Wen, Z. (2016). Review of rail corrugation progress. *Journal of Southwest Jiaotong University*, 51(2), 264–273.
- Jin, X., Wu, Y., Liang, S., Wen, Z., Wu, X., & Wang, P. (2020). Characteristics, mechanism, influences and countermeasures of polygonal wear of high-speed train wheels. *Journal of Mechanical Engineering*, 56(16), 118–136. doi: [10.3901/jme.2020.16.118](https://doi.org/10.3901/jme.2020.16.118).
- Jun, S., & Park, J. (2020). Development of a novel fatigue damage model for Gaussian wide band stress responses using numerical approximation methods. *International Journal of Naval Architecture and Ocean Engineering*, 12, 755–767. doi: [10.1016/j.ijnaoe.2020.09.005](https://doi.org/10.1016/j.ijnaoe.2020.09.005).
- Kang, X., Chen, G., Song, Q., Dong, B., Zhang, Y., & Dai, H. (2022). Effect of wheelset eccentricity on the out-of-round wheel of high-speed trains. *Engineering Failure Analysis*, 131, 105816. doi: [10.1016/j.engfailanal.2021.105816](https://doi.org/10.1016/j.engfailanal.2021.105816).
- Keegan, W. (2001). Dynamic environmental criteria. In *National Aeronautics and Space Administration Technical Handbook*, NASA-HND-7005.
- Kihm, F., Rizzi, S., Ferguson, N., & Halfpenny, A. (2013). Understanding how kurtosis is transferred from input acceleration to stress response and its influence on fatigue life. In *Proceedings of the XI International Conference on Recent Advances in Structural Dynamics*, Pisa.
- Klein, G., & Piersol, A. (1965). The development of vibration test specifications for spacecraft application. In *Measurement Analysis Corp Los Angeles Ca*.
- Knothe, K., & Grassie, S. (1993). Modelling of railway track and vehicle/track interaction at high frequencies. *Vehicle System Dynamics*, 22(3-4), 209–262. doi: [10.1080/00423119308969027](https://doi.org/10.1080/00423119308969027).
- Kurzeck, B. (2011). Combined friction induced oscillations of wheelset and track while curving of metros and their influence on corrugation. *Wear*, 271(1-2), 299–310. doi: [10.1016/j.wear.2010.10.049](https://doi.org/10.1016/j.wear.2010.10.049).
- Langer, B. (1937). Fatigue failure from stress cycles of varying amplitude. *American Society of Mechanical Engineers Journal of Applied Mechanics*, 59, A160–A162.
- Leis, B. (1988). A nonlinear history-dependent damage model for low cycle fatigue. *Transactions of the American Society of Mechanical Engineers International*, 143–159.
- Li, L., Xiao, X., & Jin, X. (2011). Interaction of subway LIM vehicle with ballasted track in polygonal wheel wear development. *Acta Mechanica Sinica*, 27(2), 297–307. doi: [10.1007/s10409-011-0427-y](https://doi.org/10.1007/s10409-011-0427-y).
- Li, W., Wang, H., Wen, Z., Du, X., Wu, L., Li, X., & Jin, X. (2016). Investigation into mechanism of metro rail corrugation using experimental and theoretical methods. *Proceedings of the Institution of Mechanical Engineers, Part F: Journal of Rail and Rapid Transit.*, 230(4), 1025–1039. doi: [10.1177/0954409715596182](https://doi.org/10.1177/0954409715596182).
- Li, F., Wu, P., Zeng, J., Liu, C., & Wu, H. (2019). Vibration fatigue dynamic stress simulation under multi-load input condition: Application to metro lifeguard. *Engineering Failure Analysis*, 99, 141–152. doi: [10.1016/j.engfailanal.2019.02.024](https://doi.org/10.1016/j.engfailanal.2019.02.024).

- Liao, X., Yi, C., Zhang, Y., Ou, F., Chen, Z., & Lin, J. (2022). A simulation investigation on the effect of wheel-polygonal wear on dynamic vibration characteristics of the axle-box system. *Engineering Failure Analysis*, 139, 106513. doi: [10.1016/j.engfailanal.2022.106513](https://doi.org/10.1016/j.engfailanal.2022.106513).
- Ling, L., Li, W., Foo, E., Wu, L., Wen, Z., & Jin, X. (2017). Investigation into the vibration of metro bogies induced by rail corrugation. *Chinese Journal of Mechanical Engineering*, 30(1), 93–102. doi: [10.3901/cjme.2016.1018.121](https://doi.org/10.3901/cjme.2016.1018.121).
- Liu, X., & Zhai, W. (2014). Analysis of vertical dynamic wheel/rail interaction caused by polygonal wheels on high-speed trains. *Wear*, 314(1), 282–290. doi: [10.1016/j.wear.2013.11.048](https://doi.org/10.1016/j.wear.2013.11.048).
- Liu, S., Yang, G., Xiao, S., Yang, B., & Zhu, T. (2019). Comparative analysis of fatigue strength of welded frame based on UIC and JIS standards. *Electric Drive for Locomotives*, 6, 91–94.
- Liu, P., Yang, S., & Liu, Y. (2022). Full-scale test and numerical simulation of wheelset-gear box vibration excited by wheel polygon wear and track irregularity. *Mechanical Systems and Signal Processing*, 167, 108515. doi: [10.1016/j.ymsp.2021.108515](https://doi.org/10.1016/j.ymsp.2021.108515).
- Liu, X., & Zhai, W. (2014). Analysis of vertical dynamic wheel/rail interaction caused by polygonal wheels on high-speed trains. *Wear*, 314(1), 282–290.
- Lotsberg, I. (2005). Background for revision of DNV-RP-C203 fatigue analysis of offshore steel structure. In *24th International Conference on Offshore Mechanics and Arctic Engineering*, ASME, Halkidiki, Paper No. OMAE2005-67549.
- Low, Y. (2014). A simple surrogate model for the rainflow fatigue damage arising from processes with bimodal spectra. *Marine Structures*, 38, 72–88. doi: [10.1016/j.marstruc.2014.06.005](https://doi.org/10.1016/j.marstruc.2014.06.005).
- Ma, C., Gao, L., Cui, R., & Xin, T. (2021). The initiation mechanism and distribution rule of wheel high-order polygonal wear on high-speed railway. *Engineering Failure Analysis*, 119, 104937. doi: [10.1016/j.engfailanal.2020.104937](https://doi.org/10.1016/j.engfailanal.2020.104937).
- Marco, S., & Starkey, W. (1954). A concept of fatigue damage. *Transactions of the American Society of Mechanical Engineers*, 76(4), 627–632. doi: [10.1115/1.4014922](https://doi.org/10.1115/1.4014922).
- Miles, J. (1954). On structural fatigue under random loading. *Journal of the Aeronautical Sciences*, 21(11), 753–762. doi: [10.2514/8.3199](https://doi.org/10.2514/8.3199).
- MIL-STD-810F (2008). Test method standard for environmental engineering considerations and laboratory tests. In *United States of America: Department of Defence*.
- Miner, M. (1945). Cumulative damage in fatigue. *Journal of Applied Mechanics*, 12(3), A159–A164. doi: [10.1115/1.4009458](https://doi.org/10.1115/1.4009458).
- Morys, B. (1998). Enlargement of out-of-round wheel profiles on high speed trains. *Journal of Sound and Vibration*, 5(227), 965–978. doi: [10.1006/jsvi.1999.2055](https://doi.org/10.1006/jsvi.1999.2055).
- Muñiz-Calvente, M., Álvarez-Vázquez, A., Pelayo, F., Aenlle, M., Garcia-Fernandez, N., & Lamela-Rey, M. (2022). A comparative review of time- and frequency-domain methods for fatigue damage assessment. *International Journal of Fatigue*, 163, 107069. doi: [10.1016/j.ijfatigue.2022.107069](https://doi.org/10.1016/j.ijfatigue.2022.107069).
- Niu, X., Li, G., & Lee, H. (1987). Hardening law and fatigue damage of a cyclic hardening metal. *Engineering Fracture Mechanics*, 26(2), 163–70. doi: [10.1016/0013-7944\(87\)90194-9](https://doi.org/10.1016/0013-7944(87)90194-9).
- OH, B. (1910). The exponential law of endurance tests. *Proceedings of American Social Test Mater*, 10, 625–630.
- Ortiz, K., & Chen, N. (1987). Fatigue damage prediction for stationary wideband processes. In *Fifth International Conference on Applications of Statistics and Probability in Soil and Structural Engineering*.
- Palmgren, A. (1924). Die lebensdauer von kugellagern. *Verfahrenstechnik Berlin*. 68, 339-S341.
- Palmieri, M., Cesnik, M., Slavic, J., Cianetti, F., & Boltezar, M. (2017). Non-Gaussianity and Non-Stationarity in vibration fatigue. *International Journal of Fatigue*, 97, 9–19. doi: [10.1016/j.ijfatigue.2016.12.017](https://doi.org/10.1016/j.ijfatigue.2016.12.017).
- Park, J., Choung, J., & Kim, K. (2014). A new fatigue prediction model for marine structures subject to wide band stress process. *Ocean Engineering*, 76, 144–151. doi: [10.1016/j.oceaneng.2013.11.002](https://doi.org/10.1016/j.oceaneng.2013.11.002).

- Peng, B., Iwnicki, S., Shackleton, P., Crosbee, D., & Zhao, Y. (2019). The influence of wheelset flexibility on polygonal wear of locomotive wheels. *Wear*, 432, 102917. doi: [10.1016/j.wear.2019.05.032](https://doi.org/10.1016/j.wear.2019.05.032).
- Peng, L., Han, J., Chu, D., Gao, Y., Liu, Z., & Xiao, X. (2019). Analysis of abnormal vibration characteristics and causes of vertical block in high-speed EMU. *Journal of Mechanical Engineering*, 55(12), 121–127. doi: [10.3901/jme.2019.12.121](https://doi.org/10.3901/jme.2019.12.121).
- Popp, K., Kruse, H., & Kaiser, I. (1991). Vehicle-track dynamics in the mid-frequency range. *Vehicle System Dynamics*, 31(5-6), 423–464. doi: [10.1076/vesd.31.5.423.8363](https://doi.org/10.1076/vesd.31.5.423.8363).
- Qu, S., Zhu, B., Zeng, J., Dai, H., & Wu, P. (2020). Experimental investigation for wheel polygonisation of high-speed trains. *Vehicle System Dynamics*, 59(10), 1573–1586. doi: [10.1080/00423114.2020.1772984](https://doi.org/10.1080/00423114.2020.1772984).
- Ren, Z., Sun, S., & Li, Q. (2010). Axle spring load test and dynamic characteristics analysis of high speed EMU. *Journal of Mechanical Engineering*, 46(10), 109–115. doi: [10.3901/jme.2010.10.109](https://doi.org/10.3901/jme.2010.10.109).
- Ren, Z., Zhao, Y., Li, Y., Wang, B., & Wu, Y. (2022). Load and damage characteristics of the traction and brake devices of bogie of high speed EMU. *Journal of Mechanical Engineering*, 58(12), 151–158.
- Rice, S. (1944). Mathematical analysis of random noise. *Bell System Technical Journal*, 23(3), 282–332. doi: [10.1002/j.1538-7305.1944.tb00874.x](https://doi.org/10.1002/j.1538-7305.1944.tb00874.x).
- Rizzi, S., Przekop, A., & Turner, T. (2011). On the response of a nonlinear structure to high kurtosis non-Gaussian random loadings. In *Proceedings of the 8th International Conference on Structural Dynamics*, Leuven. European Dynamics 2011.
- Sakai, S., & Okamura, H. (1995). On the distribution of rainfall range for Gaussian random processes with bimodal PSD. *JSME International Journal. Ser. A, Mechanics and Material Engineering*, 38(4), 440–445. doi: [10.1299/jsmea1993.38.4_440](https://doi.org/10.1299/jsmea1993.38.4_440).
- Shi, H., Wang, J., Dai, H., & Wu, P. (2019). Crack mechanism and field test of the metro safety hanger. *Journal of Mechanical Engineering*, 55(6), 122–128. doi: [10.3901/jme.2019.06.122](https://doi.org/10.3901/jme.2019.06.122).
- Spangenberg, U. (2020). Variable frequency drive harmonics and inter harmonics exciting axle torsional vibration resulting in railway wheel polygonisation. *Vehicle System Dynamics*, 58(3), 404–424. doi: [10.1080/00423114.2019.1581235](https://doi.org/10.1080/00423114.2019.1581235).
- Suda, Y., Komine, H., Iwasa, T., & Terumichi, Y. (2002). Experimental study on mechanism of rail corrugation using corrugation simulator. *Wear*, 253(1-2), 162–171. doi: [10.1016/s0043-1648\(02\)00095-9](https://doi.org/10.1016/s0043-1648(02)00095-9).
- Tao, G., Wen, Z., Liang, X., Ren, D., & Jin, X. (2019). An investigation into the mechanism of the out-of-round wheels of metro train and its mitigation measures. *Vehicle System Dynamics*, 57, 1–16. doi: [10.1080/00423114.2018.1445269](https://doi.org/10.1080/00423114.2018.1445269).
- Tao, G., Wen, Z., Jin, X., & Yang, X. (2020). Polygonisation of railway wheels: A critical review. *Railway Engineering Science*, 28(4), 317–345. doi: [10.1007/s40534-020-00222-x](https://doi.org/10.1007/s40534-020-00222-x).
- Tao, G., Xie, C., Wang, H., Yang, X., Ding, C., & Wen, Z. (2020). An investigation into the mechanism of high-order polygonal wear of metro train wheels and its mitigation measures. *Vehicle System Dynamics*, 59(10), 1557–1572. doi: [10.1080/00423114.2020.1770810](https://doi.org/10.1080/00423114.2020.1770810).
- Tassilly, E., & Vincent, N. (1991). A linear model for the corrugation of rails. *Journal of Sound and Vibration*, 150(1), 25–45. doi: [10.1016/0022-460x\(91\)90400-e](https://doi.org/10.1016/0022-460x(91)90400-e).
- Torstensson, P., & Schilke, M. (2013). Rail corrugation growth on small radius curves—measurements and validation of a numerical prediction model. *Wear*, 303(1-2), 381–396. doi: [10.1016/j.wear.2013.03.029](https://doi.org/10.1016/j.wear.2013.03.029).
- Tovo, R. (2002). Cycle distribution and fatigue damage under broadband random loading. *International Journal of Fatigue*, 24(11), 1137–1147. doi: [10.1016/s0142-1123\(02\)00032-4](https://doi.org/10.1016/s0142-1123(02)00032-4).
- Vila, P., Baeza, L., Martínez-Casas, J., & Carballera, J. (2014). Rail corrugation growth accounting for the flexibility and rotation of the wheel set and the non-Hertzian and non-steady-state effects at contact patch. *Vehicle System Dynamics*, 52(1), 92–108. doi: [10.1080/00423114.2014.881513](https://doi.org/10.1080/00423114.2014.881513).

- Wang, Y., & Wu, X. (2020). The growth and mitigation of rail corrugation due to vibrational interference between moving wheels and resilient track. *Vehicle System Dynamics*, 58(8), 1257–1284. doi: [10.1080/00423114.2019.1616099](https://doi.org/10.1080/00423114.2019.1616099).
- Wang, C., Bai, J., Wan, F., & Yan, G. (2011). Review of statistical induction analysis methods on aircraft vibration test data. *Procedia Environmental Sciences*, 10, 825–830. doi: [10.1016/j.proenv.2011.09.133](https://doi.org/10.1016/j.proenv.2011.09.133).
- Wang, W., Wang, Y., Sun, S., Liang, S., Sullivan, P. G., & Springer, J. E. (2015). Long-term load spectrum test of high-speed train bogie. *Journal of Southwest Jiaotong University*, 50(1), 84–89. doi: [10.1016/j.expneurol.2014.12.018](https://doi.org/10.1016/j.expneurol.2014.12.018).
- Wang, Z., Zhang, W., Yin, Z., Cheng, Y., Huang, G., & Zou, H. (2019). Effect of vehicle vibration environment of high-speed train on dynamic performance of axle box bearing. *Vehicle System Dynamics*, 57(4), 543–563. doi: [10.1080/00423114.2018.1473615](https://doi.org/10.1080/00423114.2018.1473615).
- Wang, Z., Cheng, Y., Mei, G., Zhang, W., Huang, G., & Yin, Z. (2020). Torsional vibration analysis of the gear transmission system of high-speed trains with wheel defects. *Proceedings of the Institution of Mechanical Engineers, Part F: Journal of Rail and Rapid Transit*, 234(2), 123–133. doi: [10.1177/0954409719833791](https://doi.org/10.1177/0954409719833791).
- Wang, B., Xie, S., Jiang, C., Song, Q., Sun, S., & Wang, X. (2020). An investigation into the fatigue failure of metro vehicle bogie frame. *Engineering Failure Analysis*, 118, 104922. doi: [10.1016/j.engfailanal.2020.104922](https://doi.org/10.1016/j.engfailanal.2020.104922).
- Wang, W., Bai, J., Wu, S., Zheng, J., & Zhou, P. (2020). Experimental investigations on the effects of fatigue crack in urban metro welded bogie frame. *Applied Sciences*, 10(4), 1537. doi: [10.3390/app10041537](https://doi.org/10.3390/app10041537).
- Wen, Z., Tao, G., Zhao, X., Wei, L., & Jin, X. (2023). Wear and RCF problems of metro wheel/rail systems: Phenomena, causes and countermeasures in China. *Wear*, 534-535, 205118. doi: [10.1016/j.wear.2023.205118](https://doi.org/10.1016/j.wear.2023.205118).
- Wolfsteiner, P. (2017). Fatigue assessment of non-stationary random vibrations by using decomposition in Gaussian portions. *International Journal of Mechanical Sciences*, 127, 10–22. doi: [10.1016/j.ijmecsci.2016.05.024](https://doi.org/10.1016/j.ijmecsci.2016.05.024).
- Wolfsteiner, P., & Breuer, W. (2013). Fatigue assessment of vibrating rail vehicle bogie components under non-Gaussian random excitations using power spectral densities. *Journal of Sound and Vibration*, 332(22), 5867–5882. doi: [10.1016/j.jsv.2013.06.012](https://doi.org/10.1016/j.jsv.2013.06.012).
- Wirsching, P., & Light, M. (1980). Fatigue under wide band random stresses. *Journal of the Structural Division*, 106(7), 1593–1607. doi: [10.1061/jsdeag.0005477](https://doi.org/10.1061/jsdeag.0005477).
- Wu, T. (2011). Effects on short pitch rail corrugation growth of a rail vibration absorber/damper. *Wear*, 271(1-2), 339–348. doi: [10.1016/j.wear.2010.10.040](https://doi.org/10.1016/j.wear.2010.10.040).
- Wu, X., Chi, M., & Wu, P. (2015). Influence of polygonal wear of railway wheels on the wheel set axle stress. *Vehicle System Dynamics*, 53(11), 1535–1554. doi: [10.1080/00423114.2015.1063674](https://doi.org/10.1080/00423114.2015.1063674).
- Wu, Y., Du, X., Zhang, H., Wen, Z., & Jin, X. (2017). Experimental analysis of the mechanism of high-order polygonal wear of wheels of a high-speed train. *Journal of Zhejiang University Science A*, 18(8), 579–592. doi: [10.1631/jzus.a1600741](https://doi.org/10.1631/jzus.a1600741).
- Wu, X., Rakheja, S., Wu, H., Qu, S., Wu, P., Dai, H., . . . Ahmed, A. (2018). A study of polygonal wheel wear through a field test programme. *Vehicle System Dynamics*, 57(6), 914–934. doi: [10.1080/00423114.2018.1494842](https://doi.org/10.1080/00423114.2018.1494842).
- Wu, X., Rakheja, S., Qu, S., Wu, P., Zeng, J., & Ahmed, A. (2018). Dynamic responses of a high-speed railway car due to wheel polygonalisation. *Vehicle System Dynamics*, 56(12), 1817–1837. doi: [10.1080/00423114.2018.1439589](https://doi.org/10.1080/00423114.2018.1439589).
- Wu, X., Rakheja, S., Cai, W., Chi, M., Ahmed, A., & Qu, S. (2019). A study of formation of high order wheel polygonalization. *Wear*, 424, 1–14. doi: [10.1016/j.wear.2019.01.099](https://doi.org/10.1016/j.wear.2019.01.099).

- Wu, H., Wu, P., Li, F., Shi, H., & Xu, K. (2019). Fatigue analysis of the gearbox housing in high-speed trains under wheel polygonization using a multibody dynamics algorithm. *Engineering Failure Analysis, 100*, 351–364. doi: [10.1016/j.engfailanal.2019.02.058](https://doi.org/10.1016/j.engfailanal.2019.02.058).
- Wu, X., Chi, M., Liu, K., Hu, F., Liang, S., Wen, Z. (2020). A bogie test bench. Sichuan province: CN110823535B, 2020-12-15.
- Wu, X., Xie, C., Liu, K., Wu, S., Wen, Z., & Mo, J. (2020). Study on high frequency vibration-induced fatigue failure of antenna beam in a metro bogie. *Engineering Failure Analysis, 133*, 105976. doi: [10.1016/j.engfailanal.2021.105976](https://doi.org/10.1016/j.engfailanal.2021.105976).
- Wu, B., Shang, Z., Pan, J., Zhang, R., Shi, P., & Xiao, P. (2022). Analysis on the formation cause for the high-order wheel polygonization of the high-speed trains based on the finite element method. *Vehicle System Dynamics, 61*, 1–18. doi: [10.1080/00423114.2022.2035777](https://doi.org/10.1080/00423114.2022.2035777).
- Wu, X., Xie, C., Liu, K., Wu, S., Wen, Z., & Mo, J. (2022). Study on high frequency vibration-induced fatigue failure of antenna beam in a metro bogie. *Engineering Failure Analysis, 133*, 105976. doi: [10.1016/j.engfailanal.2021.105976](https://doi.org/10.1016/j.engfailanal.2021.105976).
- Wu, X., Zhang, Z., Cai, W., Yang, N., Wang, W., Liu, K., . . . Liang, S. (2023). A study of the axle box ASD spectrum of high-speed rail vehicles based on field test measurements in China. *Engineering Failure Analysis, 154*, 107681. doi: [10.1016/j.engfailanal.2023.107681](https://doi.org/10.1016/j.engfailanal.2023.107681).
- Yang, Y., Xu, M., Ling, L., & Zhai, W. (2022). Polygonal wear evolution of locomotive wheels subjected to antislip control. *Wear, 500-501*, 204348. doi: [10.1016/j.wear.2022.204348](https://doi.org/10.1016/j.wear.2022.204348).
- Ye, Y., Shi, D., Krause, P., Tian, Q., & Hect, M. (2020). Wheel flat can cause or exacerbate wheel polygonization. *Vehicle System Dynamics, 58*(10), 1575–1604. doi: [10.1080/00423114.2019.1636098](https://doi.org/10.1080/00423114.2019.1636098).
- Zhai, W., Wang, K., & Cai, C. (2009). Fundamentals of vehicle–track coupled dynamics. *Vehicle System Dynamics, 47*(11), 1349–1376. doi: [10.1080/00423110802621561](https://doi.org/10.1080/00423110802621561).
- Zhai, W., Jin, X., Wen, Z., & Zhao, X. (2020). Wear problems of high-speed wheel/rail systems: Observations, causes, and countermeasures in China. *Applied Mechanics Review, 72*(6), 060801. doi: [10.1115/1.4048897](https://doi.org/10.1115/1.4048897).
- Zhang, S. (2008). Research on test and establishment method of load spectrum for high speed train bogie. *Scientia Sinica (Technologica): Series E, 38*(11), 1805–1814.
- Zhang, J., Han, G., Xiao, X., Wang, R., Zhao, Y., & Jin, X. (2014). Influence of wheel polygonal wear on interior noise of high-speed trains. *Journal of Zhejiang University Science A, 15*(12), 1002–1018.
- Zhang, B., Tan, A., & Lin, J. (2016). Gearbox fault diagnosis of high-speed railway train. *Engineering Failure Analysis, 66*, 407–420. doi: [10.1016/j.engfailanal.2016.04.020](https://doi.org/10.1016/j.engfailanal.2016.04.020).
- Zhang, F., Ping, B., & Wu, X. (2018). Effects of wheel polygonalization on axle box for high speed train. *Journal of Vibration, Measurement & Diagnosis, 38*(5), 1063–1068+1088.
- Zhao, W., & Baker, M. (1992). On the probability density function of rainflow stress range for stationary Gaussian processes. *International Journal of Fatigue, 14*(2), 121–135. doi: [10.1016/0142-1123\(92\)90088-t](https://doi.org/10.1016/0142-1123(92)90088-t).
- Zhao, X., Chen, G., Lv, J., Zhang, S., Wu, B., & Zhu, Q. (2019). Study on the mechanism for the wheel polygonal wear of high-speed trains in terms of the frictional self-excited vibration theory. *Wear, 426-427*, 1820–1827. doi: [10.1016/j.wear.2019.01.020](https://doi.org/10.1016/j.wear.2019.01.020).
- Zhou, C., Chi, M., Wen, Z., Wu, X., Cai, W., Dai, L., . . . Li, M. (2020). An investigation of abnormal vibration – induced coil spring failure in metro vehicles. *Engineering Failure Analysis, 108*, 104–238. doi: [10.1016/j.engfailanal.2019.104238](https://doi.org/10.1016/j.engfailanal.2019.104238).
- Zorman, A., Slavič, J., & Boltezar, M. (2023). Vibration fatigue by spectral methods—a review with open-source support. *Mechanical Systems and Signal Processing, 190*, 110149. doi: [10.1016/j.ymssp.2023.110149](https://doi.org/10.1016/j.ymssp.2023.110149).

Zou, H., Wu, Q., & Sun, S. (2016). Study on intercity train load spectrum distribution estimation and calibration methods based on load demarcation. *Journal of the China Railway Society*, 38(10), 27–33.

Zou, H., Wu, Q., & Sun, S. (2021). Research on load test spectrum of EMU car bogies based on damage consistency. *Chinese Journal of Theoretical and Applied Mechanics*, 53(1), 115–125.

Further reading

Cui, X., Chen, G., Zhao, J., Yan, W., Ouyang, H., & Zhu, M. (2017). Field investigation and numerical study of the rail corrugation caused by frictional self-excited vibration. *Wear*, 376-377, 1919–1929. doi: [10.1016/j.wear.2017.01.089](https://doi.org/10.1016/j.wear.2017.01.089).

DVS1612 (2014). *Design and endurance strength evaluation for welded steel joints in railway vehicle construction*. Germany: German Association for Welding and Related Procedures.

EN 13749 (2011). Railway applications - wheelsets and bogies - method of specifying the structural requirements of bogie frames.

ERRI B12/RP 17 (1997). Programme of tests to be carried out on wagons with steel underframe and body structure.

GJB/Z 126-99 (2000). The inductive methods for environmental measured data of vibration and shock.

IEC 61373 (2010). Railway applications - impact and vibration testing of locomotive and locomotive equipment.

JIS E4207 (2004). Truck frames for railway rolling stock-General rules for design.

JIS E4208 (1988). Test methods of static load for truck frames and truck bolsters of railway rolling stock.

RTCA DO-160G (1975). *Environmental conditions and test procedures for airborne equipment*. U.S. Department of Transportation Circular. USA: Federal Aviation Administration.

Tao, G., Wang, L., Wen, Z., Guan, Q., & Jin, X. (2018). Measurement and assessment of out-of-round electric locomotive wheels. *Proceedings of the Institution of Mechanical Engineers, Part F: Journal of Rail and Rapid Transit*, 232(1), 275–287. doi: [10.1177/0954409716668210](https://doi.org/10.1177/0954409716668210).

Tao, G., Wang, L., Wen, Z., Guan, Q., & Jin, X. (2018). Experimental investigation into the mechanism of the polygonal wear of electric locomotive wheels. *Vehicle System Dynamics*, 56(6), 883–899. doi: [10.1080/00423114.2017.1399210](https://doi.org/10.1080/00423114.2017.1399210).

Tao, G., Liu, X., Wen, Z., & Jin, X. (2021). Formation process, key influencing factors, and countermeasures of high-order polygonal wear of locomotive wheels. *Journal of Zhejiang University Science F*, 21(1), 70–84. doi: [10.1631/jzus.a2000081](https://doi.org/10.1631/jzus.a2000081).

UIC Code 515-4 (1993). *Passenger rolling stock: Trailer bogies-running gear: Bogie frame structure strength tests*. International Union of Railways.

UIC Code 615-4 (2003). *Motive power units- bogies and running gear- Bogie frame structure strength tests*. International Union of Railways.

Wu, Y., Wang, J., & Liu, M. (2002). Polygonal wear mechanism of high-speed wheels based on full-size wheel-rail roller test rig. *Wear*, 494–495.

Yang, Y., Ling, L., Wang, C., Liu, Z., Wang, K., & Zhai, W. (2020). Wheel/rail dynamic interaction induced by polygonal wear of locomotive wheels. *Vehicle System Dynamics*, 60(1), 211–235. doi: [10.1080/00423114.2020.1807572](https://doi.org/10.1080/00423114.2020.1807572).

Corresponding author

Xingwen Wu can be contacted at: xingwen_wu@163.com

For instructions on how to order reprints of this article, please visit our website:

www.emeraldgrouppublishing.com/licensing/reprints.htm

Or contact us for further details: permissions@emeraldinsight.com